iScience

CellPress
OPEN ACCESS

Article

Programmable modulation of ribosomal frameshifting by mRNA targeting CRISPR-Cas12a system

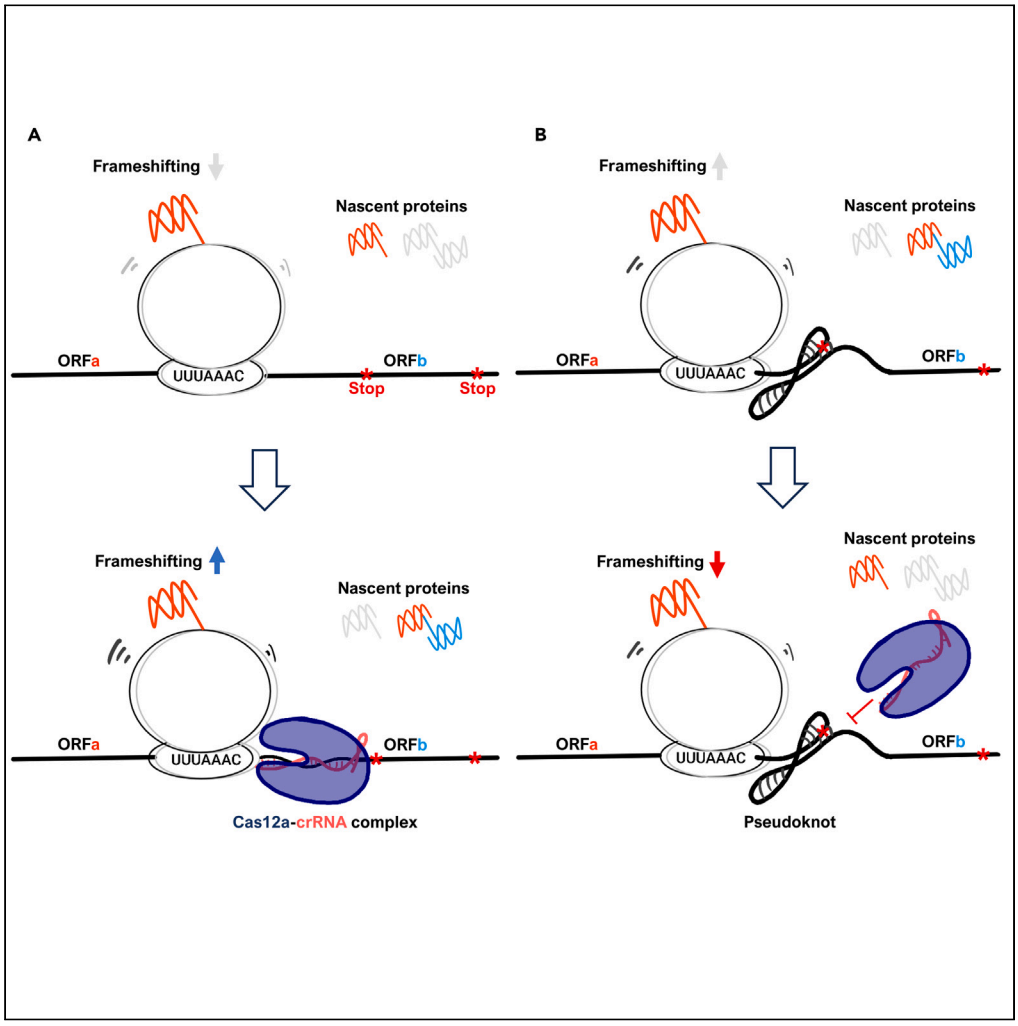

Shih-Hong Huang, Shih-Cheng Chen, Tsu-Ying Wu, Cheng-Yao Chen, Chien-Hung Yu

chienhung_yu@mail.ncku.edu.tw

Highlights

Cas12a-crRNA complex specifically binds RNA targets without triggering RNA cleavage

Cas12a-crRNA complex promotes efficient −1 PRF in a site-specific manner

Mechanistically, Cas12a-crRNA slows down ribosome elongation to stimulate −1 PRF

Cas12a-crRNA disrupts PK structure, resulting in substantial suppression of −1 PRF

Huang et al., iScience 26, 108492
December 15, 2023
https://doi.org/10.1016/j.isci.2023.108492

iScience

CellPress
OPEN ACCESS

Article

Programmable modulation of ribosomal frameshifting by mRNA targeting CRISPR-Cas12a system

Shih-Hong Huang,[1,2] Shih-Cheng Chen,[1,3] Tsu-Ying Wu,[4] Cheng-Yao Chen,[4,5] and Chien-Hung Yu[1,2,6,*]

SUMMARY

Minus 1 programmed ribosomal frameshifting (−1 PRF) is a conserved translational regulation event essential for critical biological processes, including the severe acute respiratory syndrome coronavirus 2 (SARS-CoV-2) replication. Efficient *trans*-modulation of the structured RNA element crucial to −1 PRF will endow the therapeutic application. Here, we demonstrate that CRISPR RNA can stimulate efficient −1 PRF. Assembled CRISPR-Cas12a, but not CRISPR-Cas9, complex further enhances −1 PRF efficiency through its higher capacity to stall translating ribosomes. We additionally perform CRISPR-Cas12a targeting to impair the SARS-CoV-2 frameshifting pseudoknot structure via a focused screening. We demonstrate that targeting CRISPR-Cas12a results in more than 70% suppression of −1 PRF *in vitro* and about 50% suppression in mammalian cells. Our results show the expanded function of the CRISPR-Cas12 system in modulating −1 PRF efficiency through stalling ribosomes and deforming frameshifting stimulatory signals, which could serve as a new strategy for future coronavirus pandemics.

INTRODUCTION

Canonical protein synthesis initiates from the start to the stop codon on an mRNA; during the journey, the translating ribosome moves one codon at a time[1] to faithfully decode the message, with only a small chance of making a spontaneous decoding error (1 per 10^4 codons).[2] However, dedicated signals embedded in the mRNAs can alter the meaning of genetic code or redirect the linear readout mechanism of ribosomes, a phenomenon called recoding.[3] These intrinsically designated signals dramatically "mobilize" the genetic code to increase the frequency of codon redirecting or redefinition to hundreds- or thousands-fold; therefore, the recoding events are considered programmed. Several programmed recoding mechanisms exist, including programmed ribosomal frameshifting (PRF), translational bypassing, and stop codon readthrough.[4,5] Among these translational recoding events, PRF is one of the most extensively studied mechanisms.[6] Various types of PRF were reported.[7–9] PRF is further classified based on the ribosome movement direction relative to the 5′ end of the mRNA, in the forward (+) or reverse (−) direction, and the number of nucleotides that ribosome slips. In the +1 PRF event, the ribosome slips by 1-nt in the 3′ direction on a specific shift-prone sequence, namely a slippery sequence, followed by resuming translation in the alternative reading frame to synthesize a new polypeptide with the altered C-terminal end. +1 PRF was first identified in the transposable element Ty912 of yeast.[10] Later, cellular genes in prokaryotes, *prfB*, and eukaryotes, *OAZ*, were identified to use +1 PRF for their protein synthesis.[11] Naturally occurring −2 PRF was identified for synthesizing the porcine reproductive and respiratory syndrome virus (PRRSV) nsp2TF protein, a critical protein for viral replication.[8] −1 PRF, for which the translating ribosome slips 1-nt back to the 5′ end, is the most widespread ribosomal shifting mechanism and is conserved through evolution.[6,12–14] In addition to a handful of prokaryotic and eukaryotic cellular genes, −1 PRF is predominantly found in viral genomes.[6] The viruses utilize −1 PRF to increase their genome coding capacity and to define the stoichiometry of synthesized proteins critical for virus propagation. Particular attention was directed to major human pathogenic viruses, including human immunodeficiency virus (HIV) and severe acute respiratory syndrome coronavirus (SARS-CoV). It was shown that the interference with −1 PRF efficiency leads to the restriction of replication of both viruses,[15–17] highlighting the therapeutic potential to target −1 PRF.

In general, −1 PRF is facilitated by three *cis*-acting regulatory elements: a heptameric slippery sequence, a downstream structured frameshifting stimulatory signal (FSS) (a hairpin, a pseudoknot (PK), or a G-quadruplex), and a spacer (usually between 5 and 9 nt in length) between them.[18–21] The slippery sequence, where the ribosome slips, follows a specific motif of X_XXY_YYZ (the underscore indicates the 0-frame), where X can be any nucleotide, Y represents adenine or uridine, and Z can be any nucleotide except for guanine. This motif allows P-site

[1]Department of Biochemistry and Molecular Biology, College of Medicine, National Cheng Kung University, Tainan, Taiwan
[2]Institute of Basic Medical Sciences, College of Medicine, National Cheng Kung University, Tainan, Taiwan
[3]National Institute of Cancer Research, National Health Research Institutes, Tainan, Taiwan
[4]YD BioLabs, Inc., Hsinchu, Taiwan
[5]School of Medical Laboratory Science and Biotechnology, Taipei Medical University, Taipei, Taiwan
[6]Lead contact
*Correspondence: chienhung_yu@mail.ncku.edu.tw
https://doi.org/10.1016/j.isci.2023.108492

and A-site tRNAs to re-pair to mRNA upon −1 shift due to the potential mRNA-tRNA mismatching in the wobble position.[18] The FSS downstream of the slippery sequence represents a kinetic barrier, pausing the elongating ribosome and stimulating −1 PRF during the translocation step.[22–24] Consequently, the mechanical stability of the pseudoknot FSS was shown to correlate with frameshifting efficiency.[25] Regarding hairpin FSS, thermodynamic stability is a general proxy for frameshifting efficiency.[26,27] Moreover, the intrinsic dynamic nature of the FSS structure was proposed to regulate frameshifting efficiency.[28] The length of the spacer determines the correct positioning of the stimulatory signal when the ribosome is on the slippery sequence to obtain optimal frameshifting efficiency.[20] The slip site-upstream elements were also found to regulate −1 PRF efficiency in prokaryotes[29] and in SARS-CoV.[30]

Although early reports showed that *trans*-acting factors could regulate +1 PRF efficiency,[11,31–33] −1 PRF was long considered to be predominantly regulated by RNA *cis*-acting elements[34] until a groundbreaking observation that the PRRSV nonstructural protein nsp1β transactivates −1 and −2 PRF through a slip site-downstream cytidine-rich sequence that is unable to form a stable secondary structure.[8,35] A latter study uncovered that the interaction of nsp1β and the cytidine-rich element is mediated by host poly-cytidine binding proteins,[36] presumably creating a complex to mimic the FSS to promote efficient −1 PRF. This finding opens the possibility that viral or host factors may selectively, directly or indirectly, bind *cis-elements* to regulate −1 PRF efficiency. Two host protein products of interferon (IFN)-stimulated genes, Shiftless (SHFL)[37] and the short isoform of zinc-finger antiviral protein (ZAP-S),[38] were reported to inhibit −1 PRF through the interaction with frameshifting signals. However, the specificity of this protein-frameshifting signal remains to be established.[39] More direct evidence of protein-frameshifting signal interaction is from two 2A proteins from the *Cardiovirus*. The 2A proteins of encephalomyocarditis virus (EMCV) and Theiler's murine encephalomyelitis virus (TMEV) were shown to bind putative pseudoknots to promote −1 PRF via 2A protein mediated-pseudoknot stabilization.[40–42] However, the molecular basis of the 2A protein-pseudoknot interaction remains to be determined.

In addition to *trans*-acting factors, we and others demonstrated that antisense oligonucleotides (ASOs) that bind to the specific distance downstream of slippery sequence can effectively induce +1[43] and −1 PRF,[26,44,45] providing the evidence that stable duplex is sufficient to pause translating ribosomes to shift their reading frame. The results implicate that ASO can regulate −1 PRF efficiency through the sequence-specific modulation of RNA structure formation/deformation. Further inspired by the naturally occurring protein/mRNA complex-stimulated −1 PRF,[35,41,42] we hypothesized that the protein-ASO complex may enhance the regulatory capacity of ASO in −1 PRF. The powerful CRISPR/CRISPR-associated (Cas) system, which can mimic protein-ASO complexes, offers the possibility to test this hypothesis. The well-characterized and programmable nature of the CRISPR/Cas system makes it the top candidate. For three major CRISPR/Cas systems,[46] including Cas9, Cas12a, and Cas13, we considered Cas12a is the most appropriate protein for our purpose with two primary reasons: (1) compared to Cas9, the Cas12 crRNA scaffold is in the 5′ end, which is opposite to the translation direction, that makes the RNA duplexes directly exposed to the translating ribosomes; (2) the intrinsic RNA degradation activity of Cas13 may result in unexpected RNA turnover to bias results interpretation.

In this study, we show that the Cas12a-CRISPR RNA (crRNA) complex can bind to the target mRNA without noticeable riboendonuclease activity. Targeting the Cas12a-crRNA complex to the slip site downstream region promotes about 2.5-fold more −1 PRF than the antisense crRNA alone in rabbit reticulocyte lysate (RRL). Mechanistically, the Cas12a-crRNA complex induces stronger ribosome stalling based on the established ribosomal pausing assay. The optimal spacer length between the slippery sequence and Cas12a-crRNA complex is seven nt, similar to *Cardiovirus* 2A-pseudoknot complexes. In addition, the enhanced stability of the Cas12a-crRNA complex allows efficient induction of −1 PRF of duplexes enriched with adenine (A) uracil (U) base pairs close to the ribosome. We further demonstrate the Cas12a-crRNA complex can efficiently disrupt the frameshifting pseudoknot structure of SARS-CoV, resulting in attenuated frameshifting efficiency. Based on the standardized dual luciferase assay, the most effective combination reduces SARS-CoV-2 −1 PRF efficiency by 70% *in vitro* and 50% *in cellulo*. These results demonstrate that, by learning from naturally occurring protein-directed frameshifting, Cas12a-crRNA can modulate site-specific −1 PRF efficiency. This observation provides opportunities to study the molecular basis of protein-directed −1 PRF mechanism and novel strategies for developing antiviral drugs.

RESULTS

Cas12a-crRNA complex can target mRNA without triggering RNA cleavage and stimulate efficient −1 PRF in RRL

Although the Cas12a-crRNA system harbors the mentioned advantages to test the idea of protein-ASO complex-induced −1 PRF, it is not clear if the Cas12a may trigger RNA-dependent RNA cleavage[47,48] similar to the Cas9 effector in the absence of protospacer adjacent motif (PAM).[49] Further, the non-specific *trans*-single strand DNase activity of Cas12a was reported.[48] To test the potential *cis*- or *trans*-RNase activity of Cas12a, we assembled the purified recombinant *Lachnospiraceae* sp. Cas12a-3xHA-6xHis[50] (LbCas12a-3xHA-6xHis; will be stated as Cas12a in the following text) loaded with *in vitro* synthesized crRNA followed by the incubation with the synthesized mRNA bearing the crRNA targeted sequence. We first examined the binding specificity of the Cas12a-crRNA binary to the mRNA using native agarose gel electrophoresis (Figure 1A). The results showed the addition of matched Cas12a-crRNA_v1 complex to the mRNA (Figure 1A, lane 6) results in slower migration bands than the unmatched Cas12a-crRNA_v4 complex (Figure 1A, lane 7), supporting the binding specificity of Cas12a-cRNA. An additional set of mRNA-crRNA pairs was tested and showed comparable results (Figure S1). We then performed denaturing agarose gel electrophoresis of the mRNA incubated with the targeting Cas12a-crRNA complex. The result showed the binding of Cas12a-crRNA to the mRNA did not result in noticeable degradation of targeted mRNA (Figure 1B), suggesting Cas12a will not trigger RNA-dependent RNA cleavage. We further tested if Cas12a can protect crRNA from RNase degradation, which will expand the application potential. As shown in Figure 1C, the processed crRNA[51] (crRNA*) indicated the successful binding of Cas12a, and the Cas12a-bound crRNA was stable in the presence of RNaseA.

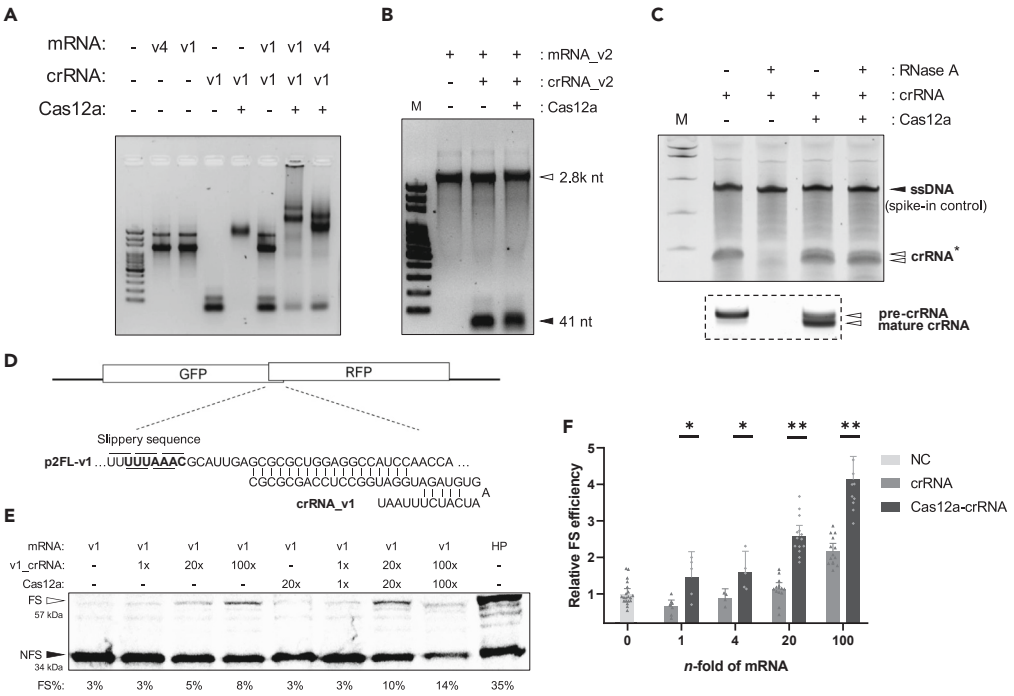

Figure 1. Cas12a-crRNA complex can specifically stimulate efficient −1 PRF without triggering RNA cleavage in RRL

(A) Representative native agarose gel showing the binding of matched mRNA_v1/crRNA_v1 and mRNA_v1/Cas12a-crRNA_v1 complex as well as the unmatched mRNA_v1/Cas12a-crRNA_v4 complex.

(B) Representative denaturing agarose gel showing the RNA cleavage assay of Cas12a.

(C) Representative urea-PAGE showing the RNase A cleavage assay of crRNA and Cas12a-crRNA. The doublet of crRNA* indicates the pre-crRNA (upper band) and mature crRNA (lower band). An additional higher-resolution image is shown in the lower bracket region. The ssDNA is the spike-in control to normalize crRNA purification.

(D) Schematic representation of the representative frameshift reporter construct (p2FL-v1). GFP is in the 0-frame while RFP -1-frame with respect to GFP. The −1 PRF is monitored by the appearance of GFP-RFP fusion product. The UUUAAAC slippery sequence is in bold. The 0-reading frame codons are indicated above the sequence; the −1 frame codons are indicated below the sequence. The sequence of the matched crRNA_v1 is shown.

(E) Representative SDS-PAGE analysis showing the [^{35}S]methionine-labeled 0-frame (non-frameshift, NFS) and -1-frame (frameshift, FS) translational products in the presence of indicated molar ratio of Cas12a protein, matched crRNA, and Cas12a-crRNA binary complex. HP is a positive control, harboring our reported frameshifting hairpin structure[27] in the p2FL vector. Radioisotope signals were recorded by storage phosphor screen followed by phosphorimager exposure. The targeted band intensity was quantified. The calculated −1 PRF efficiency is listed below the lane.

(F) Bar graph shows the relative [normalized to the negative control (NC) without crRNA or Cas12a-crRNA addition]. Data represents the mean ± SD of three or more independent replicates. Statistical analysis (paired t test): *$p < 0.05$, **$p < 0.01$.

To determine the effectiveness of the Cas12a-crRNA complex in stimulating −1 PRF, we created a dual fluorescent protein reporter (p2FL) harboring the same frameshifting context, including slippery sequence, spacer sequence, and length, and ASO-targeting sequence, as our previous reporter SF468 (Figure 1D, p2FL-v1).[26] The second fluorescent protein, red fluorescent protein (RFP), will be in-frame translated if the ribosome undergoes −1 frameshifting on the U_3A_3C slippery sequence 3′ of the green fluorescent protein (GFP) (Figure 1C). We designed and *in vitro* synthesized crRNA_v1 (detail primer sequences were listed in Table S1). The crRNA_v1 will target 7 nt downstream of the slippery sequence in p2FL-v1 to mimic the reported ASO-induced −1 PRF.[26,45] After pre-loading the v1-crRNA with recombinant Cas12a, *in vitro* translation in RRL was performed to examine the capability of crRNA and Cas12a-crRNA complex in inducing −1 PRF. By treating the crRNA_v1, the −1 PRF efficiency increases in a dose-dependent manner (Figures 1E and 1F): the −1 PRF efficiency was about 2.2-fold higher than the non-treated control in the presence of 100-fold molar excess of crRNA_v1. Interestingly, the treatment of the Cas12a-crRNA_v1 complex further increased the induced −1 PRF efficiency by about 1.5-fold at each tested concertation (Figures 1E and 1F). To determine whether the Cas12a-crRNA complex is a general strategy for efficient induction of the −1 PRF, we created another ASO-targeting sequence, 2FL-v2, with the same GC content as 2FL-v1 (Figure S2A). By targeting 2FL-v2 with the corresponding crRNA_v2, we observed a similar increment of −1 PRF efficiency as 2FL-v1 (Figures S2B–S2C). Further, when we swapped the targeting crRNA, the mismatched crRNA could not induce efficient −1 PRF even at the 500-fold molar excess concentration (Figure S2D). Similarly, adding the incompatible Cas12-crRNA complex cannot induce efficient −1 PRF (Figure S2E). These data suggest that the crRNA-induced −1 PRF is highly specific. Collectively, our data demonstrate that crRNA or Cas12a-crRNA binary complex can be a programmable and efficient *trans*-acting −1 PRF stimulator.

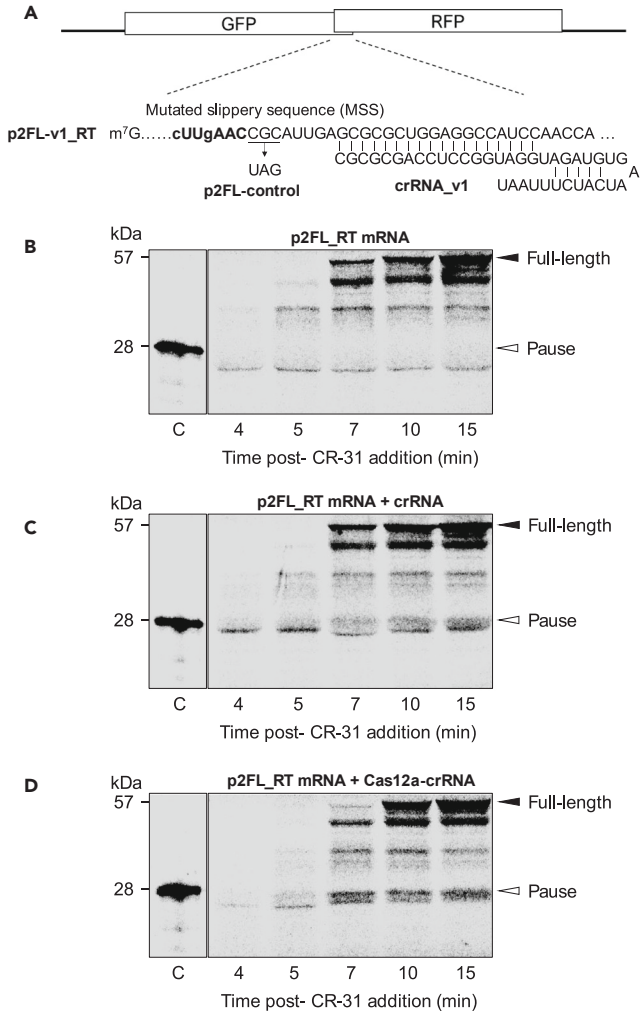

Figure 2. Both crRNA and Cas12a-crRNA complex trigger ribosome pausing

(A) Schematic representation of the ribosome pausing reporter construct (p2FL-v1-RT). The slippery sequence is mutated to a non-slippery sequence (MSS) highlighted in bold. The immediate downstream codon of the non-slippery sequence is mutated to the UAG stop codon (underlined) to construct p2FL-control. This protein product marks the expected position of crRNA or Cas12a-crRNA-induced ribosome pausing product. Refer to the legend in Figure 1 for the rest of the details.

(B–D) The mRNAs of indicated constructs were translated in RRL in the presence of [^{35}S]methionine, after 5 min further initiation was halted by the addition of CR-31, and aliquots were removed at various times and analyzed by SDS-PAGE. Lane C shows makers of ribosome pausing at the MSS. Translation reactions were supplemented with 10 pmol crRNA (50-fold molar excess to the mRNA) (C) or 10 pmol Cas12a-crRNA complex (50-fold molar excess to the mRNA) (D). Full-length and pause products are indicated by filled and empty arrowheads, respectively.

CrRNA and Cas12a-crRNA complex stimulate −1 PRF via pausing translating ribosomes

To further understand the mechanism of crRNA- and Cas12a-crRNA complex-stimulated −1 PRF, we performed a ribosome pausing assay to test if the crRNA or Cas12a-crRNA complex can pause translating ribosomes at the frameshift (FS) site (Figure 2A),[52] a mechanistic explanation for functional FSSs. To monitor the translation pausing, we mutated the slippery sequence to a non-slippery sequence (p2FL-v1_RT) to facilitate the observation of pause-then-continue translation events.[40,52] In addition, we cloned a stop codon immediately downstream of the mutated slippery sequence (p2FL-control) to obtain a protein product as the pausing marker (indicated as Pause in Figures 2B–2D). Specifically, the pausing was assessed by monitoring the [^{35}S] methionine-labeled polypeptide products during a time course in which the translation reaction was synchronized by the addition of translation initiation inhibitor CR-1-31-B,[53] 5 min after the start of the reaction. Compared to the non-treated control (Figure 2B), reactions treated with crRNA and Cas12a-crRNA complex resulted in a stronger pausing band corresponding to the ribosome decoding the slippery sequence (Figures 2C and 2D). In support of this, the amount of full-length products of non-treated and crRNA-treated conditions at 12 min after CR-1-31-B addition are more abundant than that of Cas12a-crRNA complex-treated condition (Figures 2B–2D), suggesting the translation elongation is hampered in the presence of Cas12a-crRNA complex.

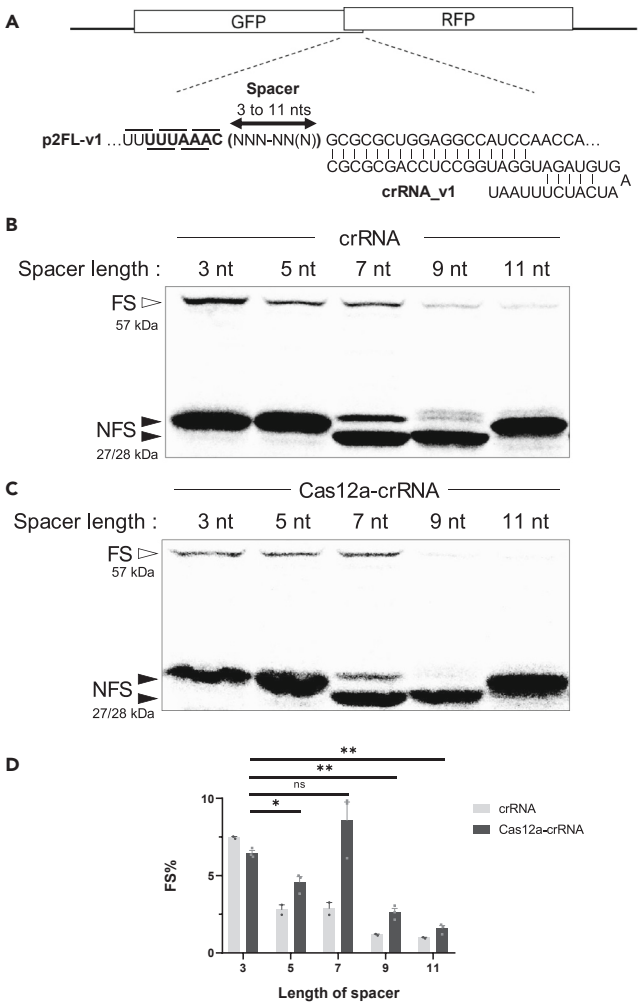

Figure 3. Determine the optimal spacer length of crRNA- and Cas12a-crRNA-induced −1 PRF

(A) Schematic representation of the −1 PRF reporter constructs based on p2FL-v1. The spacer length between the U_3A_3C slip site (in bold) and the downstream stimulator, crRNA_v1 or Cas12a- CrRNA_v1, is modified from 3 nt to 11 nt. Refer to the legend to Figure 1 for the rest of the details.

(B and C) The reporter mRNAs with indicated spacer length were translated in RRL in the presence of [^{35}S]methionine. Translation products were analyzed by SDS-PAGE followed by successive imaging and quantification. In the construct of 7 nt and 9 nt spacer length, the in-frame product (NFS) is the lower band due to their distinct reading frame caused by the designed spacer length. The shifted products (FS) are indicated. Note that, due to the varied linker sequence, the molecular weight of the FS products is slightly different (Table S2). Translation reactions were supplemented with a 100-fold molar excess of crRNA (B) or a 100-fold molar excess of Cas12a-crRNA complex (C).

(D) The bar graph shows the −1 PRF efficiency (FS%) in the presence of crRNA (light gray) or Cas12a-crRNA complex (dark gray). Data represents the mean ± SEM of three independent replicates. Statistical analysis (paired t test): ns: not significant, *p < 0.05, **p < 0.01.

The crRNA and Cas12a-crRNA complex-induced −1 PRF efficiency is spacer length dependent

It is well accepted that the spacer sequence length is critical to −1 PRF due to its role in placing the structural obstacles in the ribosomal mRNA entry channel.[20] Based on the solved Cas12a-crRNA structure, extended peptides from the targeted duplex region[54,55] may clash with translating ribosomes when the spacer length is not optimal. To better characterize the novel crRNA or Cas12a-crRNA complex-induced −1 PRF, we created constructs with spacer lengths varying from 3-nt to 11-nt while maintaining the crRNA targeting sequence (Figure 3A). The treatment of crRNA alone resulted in the highest −1 frameshifting when the spacer length is 3-nt, reminiscent to the previously reported morpholino oligonucleotides[44] (Figures 3B and 3D). However, the optimal spacer length of the Cas12a-crRNA complex is 7-nt downstream of the slippery sequence (Figures 3C and 3D), comparable to the reported 2A-pseudoknot frameshifting signals.[40–42] This longer optimal spacer length may be due to the extra molecular space occupied by the Cas12a protein. We noted that, in the construct of 7-nt and 9-nt spacer, an additional band with a larger molecular weight than the predicted non-frameshift (NFS) appeared (Figures 3B and 3C, lane 3, 4). By checking the primary sequences and searching for the size-matched +1/-2 frameshifting or stop codon readthrough product, we considered this second band may be from leaky termination. Alternatively, it could be due to alternative translation initiation. The exact reason is not clear.

Nevertheless, we estimated the −1 PRF efficiency based on the intensity of NFS and FS with the predicted molecular weight. Therefore, this unknown product did not affect our data interpretation.

To further examine the spacer length effect of CRISPR-Cas complex in −1 PRF frameshifting, we decided to test Cas9 guiding RNA (gRNA) and Cas9-gRNA complex. Catalytically dead Cas9 (dCas9) was purified to prevent targeted mRNA degradation for the following assays.[56] Because the scaffold of the CRISPR-dCas9 gRNA is in its 3′ end that may encounter translating ribosome before the ASO-mRNA duplex, this may also lead to a longer effective spacer length compared to the Cas12a crRNA. Indeed, we observed the optimal spacer length for Cas9-gRNA (gRNA_v1) is 7-nt (Figures S3A–S3B). Moreover, the dCas9-gRNA complex did not significantly enhance the stimulated −1 PRF efficiency of gRNA_1 (Figure S3C), presumably because the dCas9-gRNA complex was stripped from mRNA due to the steric hindrance when ribosomes were decoding slippery sequence.

Cas12a-crRNA complexes enhance the local stability of ASO-mRNA duplexes enriched with AU base pairs to induce efficient −1 PRF

Most of the identified frameshifting signals,[19] either a stem-loop or a pseudoknot structure, enrich G-C pairs in the bottom stem regions, especially in the first 3–4 bp of the bottom stem. The local thermodynamic stability of this region, which may reside in the mRNA entry channel upon the ribosome decoding slippery sequence, is critical to −1 PRF efficiency.[26,54] Reducing the local stability by changing a G-C to A-U base pair while maintaining the thermodynamic stability of the entire HIV frameshifting stem-loop dramatically compromises frameshifting-inducing capability.[54] We hypothesized that the Cas12a-crRNA complex could stabilize the local ASO-mRNA duplex enriched with AU base pairs to promote −1 PRF. To test this, we created constructs, based on p2FL-v1, to replace the first two nucleotides of the crRNA targeting region from 5′-GC-3′ to 5′-AU-3′ (p2FL-v3, Figure 4A) and to replace the first four nucleotides from 5′-GCGC-3′ to 5′-AUAU-3′ (p2FL-v4, Figure 4A). The corresponding crRNAs, crRNA_v3, and crRNA_v4 were *in vitro* synthesized and purified. The treatment of 100-fold molar excess of corresponding crRNAs can effectively stimulate −1 PRF on the p2FL-v1 construct (2-fold) but only leads to a marginal increase of frameshifting efficiency of 2F-v3 (1.3-fold) and 2F-v4 (1.5-fold), agreeing with previous observations[26,54] (Figures 4B and 4C). Interestingly, the treatment of Cas12a-crRNA complexes results in comparable enhancement of −1 PRF efficiency of p2FL-v3 (3.2-fold) and p2FL-v4 (2.2-fold) to p2FL-v1 (3-fold) (Figures 4B and 4C). These results indicate that the Cas12a-crRNA complexes stabilize the local stability of the ASO-mRNA duplex to make a none-stimulator duplex an efficient frameshifting signal.

Targeting crRNAs to SARS-CoV-2 frameshifting pseudoknot efficiently suppresses −1 PRF

Encouraged by our results that Cas12a-crRNA complexes can specifically anneal mRNA to induce −1 PRF, we further hypothesized that our Cas12a-crRNA complexes can target frameshifting signals in *trans* to deform their structures to alter frameshifting efficiency. Previous studies showed the *cis*-alternation of frameshifting signal structures leads to non-optimal −1 PRF efficiency, resulting in compromised replication of pathological viruses,[15,16,55,57] laying the rationale for our hypothesis. To test this, we selected the SARS-CoV-2 -1 PRF context as our model due to its significance in global public health and performed rational design of SARS-CoV-2 frameshifting pseudoknot-targeting crRNAs. Several SARS-CoV-2 frameshifting signal structures were recently proposed.[57–61] We focused on the one from Atkins' and Ban's group because the structure was obtained in the action of translation.[61] The cloned SARS-CoV-2 frameshifting context with the predicted secondary structure of frameshifting pseudoknot was shown in Figure 5A, while the sequences of rationally designed crRNAs to target the three stems (S1 to S3) of SARS-CoV-2 frameshifting pseudoknot were shown in Table 1. The GC content and the predicted thermodynamic stability based on Vienna RNA package[62] were also shown in Table 1. The targeted regions were denoted as "SS" for slippery sequence and "S" for stem, while the superscript "P" or "D" after the stem annotation indicated the slippery sequence at proximal or distal side of the stem, respectively (Figure 5B). To better observe the effect of −1 PRF suppression; we added 100-fold molar excess of crRNAs into the following *in vitro* translation assay.

Targeting the SS-proximal S1 plus S2 (crRNA_I [$S1^P$ + $S2^P$]) or SS plus SS-proximal S1 (crRNA_V [SS + $S1^P$]) showed marginal suppression of ~10% or 30%, respectively (Figures 5C and 5E). We reasoned that the mRNA targeting crRNA_I, although it may deform the native pseudoknot structure, formed a stable duplex structure that can induce efficient −1 PRF.[26,43,45] Therefore, the overall frameshifting efficiency is not compromised. The low suppressive capability of crRNA V could be due to the duplex melting by ribosomes upon translating the codons on the slip site (Figures 5A and 5B). Targeting S3 by crRNA_III showed marginal suppression (~20%) (Figures 5C and 5E), supporting the reported minor role of S3 in −1 PRF in coronaviruses.[63] In addition, the addition of crRNA_X ($S1^D$ + $S3^P$) suppressed about 30% of −1 PRF. Furthermore, CrRNA_II ($S2^P$ + $S1^D$) and crRNA_IV ($S3^D$ + $S2^D$) were designed to target S2 (Figures 5A and 5B), the formation of which was proposed to help resist ribosome unwinding of S1 to enhance −1 PRF efficiency.[64] Accordingly, crRNA II (~60% suppression) and crRNA IV (~40% suppression) were more suppressive than others. To further confirm the −1 PRF suppression is indeed due to the crRNA targeting the frameshifting pseudoknot, we performed binding assays of SARS-CoV-2 frameshifting pseudoknot-containing mRNA and crRNAs. Our data showed that the matched crRNA_VIII did bind to the target mRNA more efficiently than the non-matched crRNAs (Figures S4A–S4D).

Compared the crRNA_II and crRNA_IV, the GC content and the predicted duplex-forming thermodynamic stability of crRNA II (GC content is 59%, ΔG is −35 kcal/mol) are both better than those of crRNA IV (GC content is 50%, ΔG is −28 kcal/mol) (Table 1). It prompted us to investigate the correlation between the binding affinity and the level of SARS-CoV-2 -1 PRF suppression. Therefore, we further designed another two S2-targeting crRNAs, crRNA_VIII ($S2^D$) (GC content is 44%, ΔG is −29 kcal/mol) and crRNA_IX ($S3^D$ + $S2^D$) (GC content is 44%, ΔG = −27 kcal/mol) (Figures 5A and 5B) to test this idea. Although both crRNA VIII and crRNA IX have similar GC content and thermodynamic stability (Table 1), crRNA VIII was more suppressive (~40% suppression) than crRNA IX (~20% suppression) (Figures 5C and 5E),

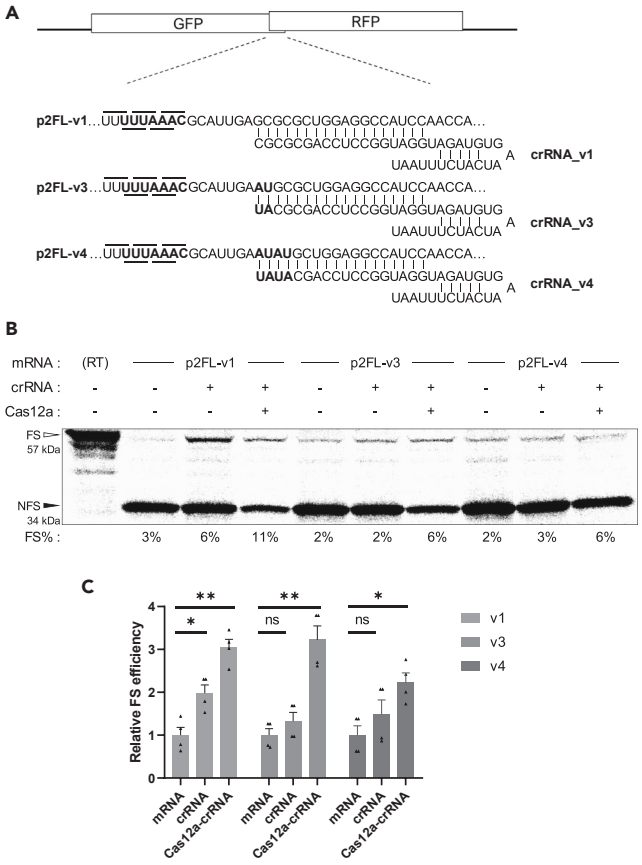

Figure 4. The formation of the Cas12a-crRNA complex enhances the capability of the otherwise inefficient crRNA −1 PRF stimulator with higher AU content

(A) Schematic representation of the major sequence context of −1 PRF reporter constructs with the matched crRNAs. Refer to the legend in Figure 1 for the rest of the details.

(B) The indicated reporter mRNAs supplemented with matched crRNA or Cas12a-crRNA were translated in RRL in the presence of [^{35}S]methionine. Translation products were analyzed by SDS-PAGE followed by successive imaging and quantification. The quantified −1 PRF efficiency of the representative gel is listed below each lane. FS: frameshifted product; NFS: in-frame product.

(C) Bar graph shows the relative −1 PRF efficiency (FS%) normalized to the control without adding crRNA or Cas12a-crRNA complex. Data represent the mean ± SEM of four independent replicates. Statistical analysis (paired t test): ns: not significant, *p < 0.05, **p < 0.01.

suggesting that the thermodynamic contribution may not be the significant factor to predict the −1 PRF suppressive effect of crRNAs, even though these crRNAs targeted similar regions of frameshifting pseudoknot. The discussion section will discuss further interpretation of crRNA-mediated −1 RPF suppression. Nevertheless, our data suggest that crRNAs can effectively target FSS to suppress −1 PRF efficiency, presumably through the deformation of the frameshifting structure.

Targeting Cas12a-crRNA complexes to SARS-CoV-2 frameshifting pseudoknot can further suppress −1 PRF

Since we found the Cas12a-crRNA complex can better stabilize the RNA duplex structure (Figure 1D), we further tested the capability of indicated crRNAs preloaded onto Cas12a proteins in suppressing −1 PRF (Figures 5D and 5E). Although Cas12a-crRNA_II, V, and X showed attenuated or similar repressive ability compared to the corresponding crRNAs, the other five Cas12a-crRNA complexes resulted in further ~20% suppression of −1 PRF, with the most effective Cas12a-crRNA_VIII suppressing ~70% of −1 PRF (Figures 5C–5E). To further confirm the specificity of Cas12a-crRNA in −1 PRF suppression, Cas12a-crRNA_VIII was incubated with the non-targeted p2FL-HP frameshifting reporter, which harbors the reported frameshifting hairpin structure,[26,27,65] in RRL. The result showed that adding Cas12a-crRNA_VIII did not affect non-targeted hairpin-induced −1 PRF (Figure S4E), suggesting that using Cas12a-crRNA complex to target frameshifting pseudoknot is specific.

We also examined the suppression using the established dual luciferase assay in RRL. The results showed similar relative suppression as our p2FL vector (Figure S5). Together, our results demonstrated that antisense crRNAs that target frameshifting signals could suppress −1 PRF, presumably through the deformation of the frameshifting structure. The suppressive effect can be enhanced by the assembled Cas12a-crRNA complex that further stabilizes the interaction with the targeted RNA.

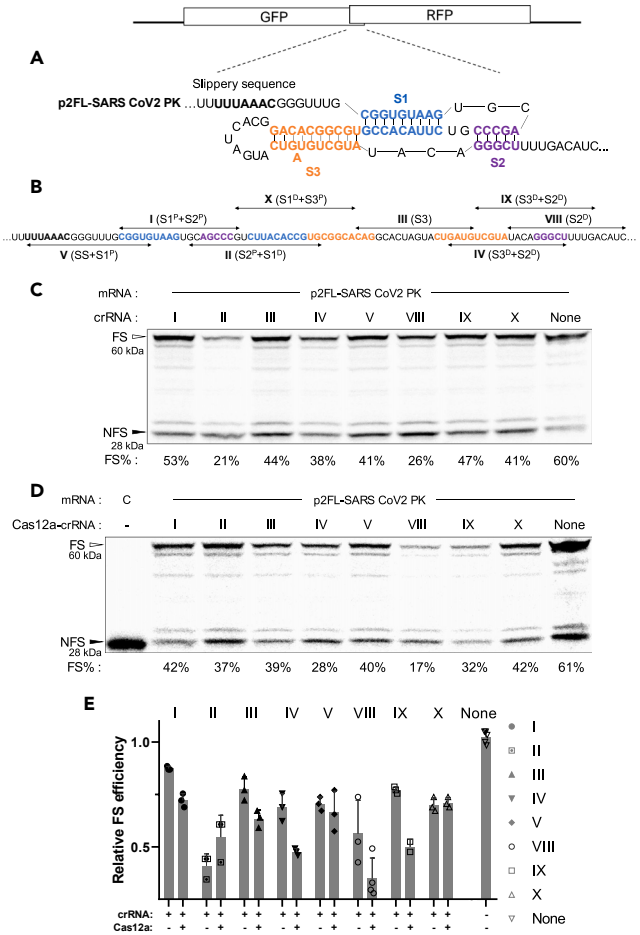

Figure 5. Deformation of SARS-CoV-2 frameshifting pseudoknot by crRNA and Cas12a-crRNA efficiently attenuate −1 PRF efficiency

(A) Schematic representation of the frameshift reporter construct harbors SARS-CoV-frameshifting pseudoknot (p2FL-SARS-CoV-2 PK). The depicted secondary structure is based on the model of Bhatt et al.[61] S denotes the stem structure. The three stems are further colored in blue (stem 1, S1), purple (stem 2, S2), and orange (stem 3, S3). Refer to the legend in Figure 1 for the rest of the details.

(B) Arrowed lines indicate the designed crRNAs, expressed as Roman numerals, targeted regions of SARS-CoV-2 frameshifting pseudoknot. The crRNA targeting region is further denoted in the bracket: SS denotes slippery sequence; S denotes stem structure; the superscript P and D indicate the proximal targeting or distal targeting, respectively.

(C and D) The reporter mRNA supplemented with indicated crRNAs (C) or Cas12a-crRNAs (D) were translated in RRL in the presence of [^{35}S]methionine. Translation products were analyzed by SDS-PAGE followed by successive imaging and quantification. The quantified −1 PRF efficiency of the representative gel is listed below each lane. FS: frameshifted product; NFS: in-frame product.

(E) Bar graph shows the relative level of −1 PRF suppression normalized to the control without adding crRNA or Cas12a-crRNA complex. Data represents the mean ± SD of three or more independent replicates. Statistical analysis (paired t test): *$p < 0.05$, **$p < 0.01$.

Efficient suppression of reporter-based SARS-CoV-2 −1 PRF by Cas12a-crRNA complex in living cells

It has been shown that *cis* or *trans* alteration of −1 PRF efficiency will suppress the replication of various viruses employing −1 PRF.[15–17,55,57,66,67] Motivated by our observations that Cas12a-crRNA complexes can efficiently suppress SARS-CoV-2 -1 PRF *in vitro*, we set forth to test the capability of crRNA and Cas12a-crRNA in suppression of SARS-CoV-2 −1 PRF in living cells. To better mimic the infection of RNA viruses, we co-transfected *in vitro* transcribed p2luc reporter mRNA harboring the SARS-CoV-2 frameshifting signal together with crRNA_VIII or Cas12a-crRNA_VIII complex. Immunofluorescence staining of transfected Cas12a-crRNA complex indicated that the complex mainly resided in the cytoplasm (Figure 6A). By measuring the dual luciferase activity after 8 h of transfection, the result showed that the treatment of crRNA_VIII alone did not lead to significant suppression of −1 PRF (Figure 6B), probably due to its degradation by endogenous RNases. In comparison, the treatment of the Cas12a-crRNA_VIII complex resulted in about 50% suppression of −1 PRF (Figure 6B). These results suggest that Cas12a enhances the crRNA in −1 PRF suppression by (1) increasing the half-life of cRNA (Figure 1C) and (2) stabilizing the interaction between crRNA and targeted mRNA (Figures 5C and 5D) in living cells. Collectively, our data showed the rationally designed Cas12a-crRNA complex can specifically and efficiently suppress −1 PRF in living cells through targeting frameshifting stimulators.

Table 1. List crRNA sequences, including the GC content and the predicted thermodynamic stability upon forming a duplex with SARS-CoV-2 frameshifting pseudoknot

GC% of antisense sequence and predicted ΔG of a heterodime

	crRNA	GC%	ΔG(kcal/mol)
I	GGUAAUUUCUACUAAGUGUAGAU CGGGCUGCACUUACACCG	67%	−28
II	GGUAAUUUCUACUAAGUGUAGAU CGGUGUAAGACGGGCUGC	59%	−35
III	GGUAAUUUCUACUAAGUGUAGAU CAUCAGUACUAGUGCCUG	50%	−28
IV	GGUAAUUUCUACUAAGUGUAGAU AGCCCUGUAUACGACAUC	50%	−28
V	GGUAAUUUCUACUAAGUGUAGAU CACCGCAAACCCGUUUAA	50%	−27
VIII	GGUAAUUCCCACUAAGUGUGGGU GAUGUCAAAAGCCCUGUA	44%	−29
IX	GGUAAUUCCCACUAAGUGUGGGU CAAAAGCCCUGUAUACGA	44%	−27
X	GGUAAUUCCUACUAAGUGUAGGU UGCCGCACGGUGUAAGAC	61%	−27

DISCUSSION

In this study, we demonstrate that the Cas12a-crRNA complex is a programmable tool to efficiently and specifically modulate −1 PRF efficiency *in vitro* and living cells. With the bound Cas12a protein, the local stability of the mRNA-crRNA duplex is further enhanced, revealed by the prolonged ribosome pausing and increased −1 PRF efficiency, reminiscent of the protein-directed −1 PRF in reported RNA viruses.[35,40] Additionally, this enhanced binding feature can compete with folded frameshifting signals to attenuate −1 PRF efficiency in living cells, implicating the therapeutic potential against pathogenic RNA viruses that require optimal −1 PRF efficiency for replication.[15–17,57,66,67,69]

Given the importance of the evolutionary conserved PRF in diverse biological functions,[6] efforts were made to predict PRF events in available genomes based on the criteria of *cis*-acting frameshifting elements.[70–72] However, these sophisticated tools cannot predict the *trans*-activated PRF events[8,40,42] that lack all three defined *cis*-acting elements. Our current data further suggest the *trans*-activated PRF events may be a more general feature: an optimal positioned RNA-protein complex guided by sense-antisense interaction can mimic the ribosome roadblock to stimulate PRF. In support of this, it was recently discovered that a small interfering RNA (siRNA)-guided Argonaute-microRNA-SGS3 complex can lead to site-specific ribosome stalling in plants[73] as well as a particular class of siRNAs that target coding regions.[74] Moreover, this idea may provide clues to understand why there are no apparent *cis*-mRNA stimulatory structures downstream of slippery sequences in a group of alphaviruses[75]: the counteracting factor of higher AU content in the potential frameshifting signal region, from 8 to 12 nt downstream of slippery sequence, could be overcome by RNA-protein complex (Figure 4). Also, it may provide potential explanation of microRNA (miRNA)-mediated ribosomal frameshifting,[76] albeit an improved reporter system contested this report.[77] Nevertheless, our data extend the scope of protein-directed ribosomal frameshifting, which is currently limited in viruses, to hint that RNA-protein complexes targeting the optimal position downstream of potential slippery sequence can trigger ribosomal frameshifting. The exploration of this may be achieved by the recently developed high-throughput approach in targeted cells.[78]

Due to the crucial role of FSS in −1 PRF, the optimal efficiency of which impacts viral replication and life cycle,[15,17,55] many studies based on the characterized structural features of FSSs to design small molecules as the antiviral drugs.[79–82] Although promising, this strategy relies on thoroughly understanding FSS structure information and extensive small molecule screening. Moreover, the fast-evolving nature of viruses may adopt different FSSs,[19,63] such as evolving human coronaviruses,[63] that lead to compromised efficacy of developed compounds. Alternatively, targeting the primary sequence by ASOs may offer the advantages of fast design and higher specificity to restrict viral pandemics and, therefore, could be a first-line therapy against emerging viruses that require PRF. Similar ideas were recently tested.[57,83] Our Cas12a-crRNA system offers additional advantages to the ASOs from these reports, which are listed in the following. (1) The chemistry of ASO, crRNA in our case, is more flexible due to the resistance to RNases by Cas12a protection (Figure 1). This may essentially eliminate the toxicity concern of modified nucleotides.[57,84] (2) The Cas12a-crRNA offers higher local stability (Figure 2) to stall translating ribosome and better capability to deform FSS (Figure 5). We speculate that both activities may be further assisted by the unique target searching feature of Cas proteins,[85] although further evidence is needed to support this hypothesis. (3) We demonstrate that, without nuclear localization sequence (NLS), Cas12a is predominantly located in the cytoplasm (Figure 6A). This cytoplasm-enriched feature can increase the effective concentration of Cas12a-crRNA to target cytosolic viral mRNA and prevent the unpredictable effect of nuclear entry ASOs.[86] Accordingly, with the recent advances in engineered virus-like particles (eVLPs) technology of *in vivo* CRISPR gene editing delivery,[87] combining our discovery with the eVLP could be a potential therapeutic agent against pathogenic HIV or SARS-CoV.

The relative lower NFS and FS band intensities were found in the experiment with the addition of 100-fold molar excess of Cas12a-crRNA complex (Figure 1E, lane 8; Figure 4B land 4, 7, 10; Figure S4E, land 1, 2). Since we demonstrated that the Cas12-crRNA complex did not cleave the target mRNA (Figure 1B), the decrease is not due to the lower mRNA concentration. Alternatively, we reasoned that, due to the relatively high concentration of Cas12a-crRNA complex (equal to 1 μM when added in a 100-fold molar excess), translating ribosomes have to remove the non-specifically attached Cas12a-crRNA complexes on the mRNA and, therefore, the translation efficiency is compromised. Nevertheless, since we estimate −1 PRF efficiency by calculating the ratio between FS (frameshifted) and NFS (non-frameshifted) products, our conclusion that the Cas12a-crRNA complex can specifically modulate −1 PRF is justified.

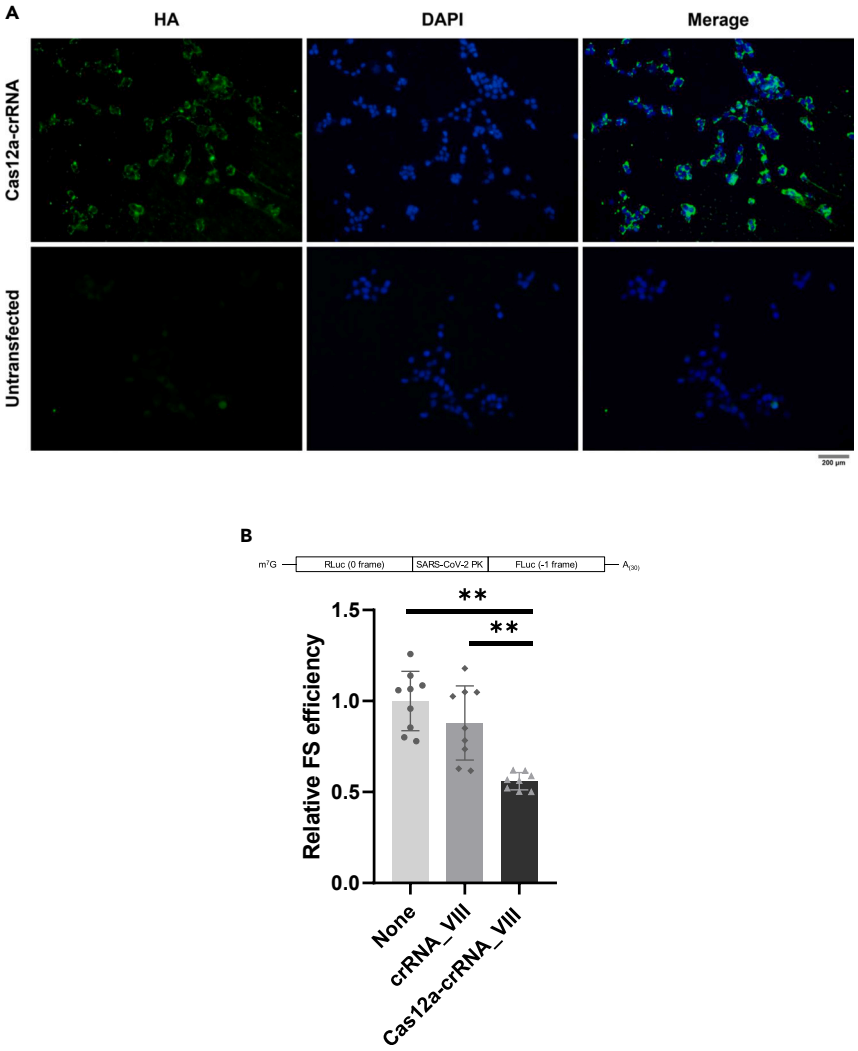

Figure 6. Cas12a-crRNA attenuates SARS-2 −1 PRF in human cells

(A) Representative images of immunofluorescence staining of HEK293T cells transfected with or without assembled Cas12a-crRNA_VIII complex using HA antibody against the C-terminal 3HA tag of recombinant Cas12a. DAPI is applied to stain nuclear DNA.

(B) *In vitro* transcribed and capped dual luciferase reporter[68] mRNA was co-transfected with none, crRNA_VIII, and Cas12a-crRNA_VIII for 8 h, followed by the measurement of luciferase activity. The bar graph shows the relative level of −1 PRF suppression normalized to the none co-transfection control. Data represent the mean ± SD of nine independent biological repeats. Statistical analysis (paired t test): **$p < 0.01$.

Although our rational-designed SARS-CoV-2 frameshifting pseudoknot-targeting crRNAs are relatively specific (Figures S4A–S4C), and these cRNAs can suppress −1 PRF (Figures 5C–5E), the level of suppression cannot be simply predicted based on crRNA binding affinity or crRNA targeting region. Take the targeting of S1, which is the critical stem to resist ribosome unwinding to induce −1 PRF,[25] as an example; although we predicted the reason for less suppressive proximal S1-targeting crRNA_I (∼10% suppression with crRNA alone and ∼30% suppression in the binary complex form) (Figure 5) is due to the formation of a stable RNA duplex upon targeting (i.e., creating a frameshifting-competent secondary structure at the optimal location[26,27,43–45]), the treatment of crRNA_X, which was designed so that it targets the distal S1 and the formed duplex should not induce -1PRF due to the non-optimal distance to the slip site, did not lead to robust suppression of −1 PRF (∼30% suppression with sole crRNA and ∼30% suppression in the binary complex form). The potential explanation for the low prediction power is that the −1 PRF efficiency readout could be affected by additional factors, such as the formation of alternative RNA structures after crRNA or Cas12-crRNA targeting in dynamic refolding processes during translation.[28,72] An observation from S2 targeting crRNAs (crRNA_II, IV, VIII, and IX) may provide a clue to design better – 1 PRF suppressor crRNAs: the 3′ end of crRNA that annealed to the flexible loop region between S1 and S2 or S2 and S3 can result in better −1 PRF suppression. We hypothesized that the accessibility of such crRNA to the structured target could be more efficient by initial targeting to the single-stranded region within the target (Figure 5A), reminiscent of DNA strand invasion.[88] Nevertheless, understanding the fraction of alternative RNA conformers[89] during translation would help predict the potency of crRNA.

During the preparation of our manuscript, a study from the Heo lab demonstrated that among the twelve crRNA-Cas13b complexes designed to target the open reading frame 1b (ORF1b) region to degrade the RNA-dependent RNA polymerase (RdRp) gene, the targeting of SARS-CoV-2 frameshifting pseudoknot is the most efficient site to inhibit SARS-CoV-2 propagation.[90] This result supports our data in two aspects: (1) −1 PRF mechanism is a promising drug target against pathogenic viruses that rely on it; (2) the CRISPR-Cas system can be applied to target compact frameshifting stimulatory structures specifically. Nonetheless, the mechanism of our Cas12-crRNA system is to disrupt the frameshifting structure instead of triggering target RNA degradation, like the Cas13b system. Therefore, our Cas12-crRNA strategy may cause more subtle side effects than the Cas13b system if the off-targeting is inevitable.[91] Because, regarding host cellular mRNA, the off-targeted Cas12a-crRNA complexes will be removed by translating ribosomes.

Limitation of the study

Although our data support that Cas12a-crRNA complexes can module −1 PRF through either enhancing the frameshift efficiency as a roadblock or inhibiting −1 PRF by disrupting the frameshifting inducing PK structure, we observe that the addition of a high concentration of Cas12a-crRNA suppresses the translation efficiency of the reporter gene in RRL. We reason that the suppression of translation efficiency comes from the accumulated roadblock effects of the Cas12a-crRNA complex along the ribosome journey of the transcript. Therefore, treating the Cas12a-crRNA complex in higher doses, exceeding μM level, may accompany the trade-off of reducing protein yield.

Additionally, in the inhibition of frameshifting PK formation experiments, the inhibitory effects of Cas12a-crRNAs are not always more effective than the corresponding crRNAs. Further, the inhibitory level cannot be simply predicted by the binding affinity of the Cas12a-crRNA-target RNA complexes. This may be due to the complicated interaction network between the Cas12a-crRNA-target RNA-ribosome, resulting in alternative folded frameshifting RNAs. Therefore, probing the dynamic RNA structures in the presence of Cas12a-crRNA during translation is critical to understanding how the Cas12a-crRNA-RNA complexes affect −1PRF.

Furthermore, in the current study, we did not investigate the mechanism of how Cas12a-crRNA specifically recognizes RNA targets. It will be interesting to explore whether the Cas12a-crRNA complex searches for RNA targets through the canonical one-dimensional diffusion mechanism.

STAR★METHODS

Detailed methods are provided in the online version of this paper and include the following:

- KEY RESOURCES TABLE
- RESOURCE AVAILABILITY
  - Lead contact
  - Materials availability
  - Data and code availability
- EXPERIMENTAL MODEL AND STUDY PARTICIPANT DETAILS
- METHOD DETAILS
  - Plasmid construction
  - *In vitro* transcription
  - Expression and purification of Cas12a
  - Expression and purification of dCas9
  - Electrophoretic mobility shift assay (EMSA)
  - Cas12a RNA cleavage activity assay
  - RNase protection assay
  - *In vitro* translation
  - Cell culture and transfection
  - Immunofluorescence assay
- QUANTIFICATION AND STATISTICAL ANALYSIS

SUPPLEMENTAL INFORMATION

Supplemental information can be found online at https://doi.org/10.1016/j.isci.2023.108492.

ACKNOWLEDGMENTS

We appreciate Professor Kung-Yao Chang (Dept. of Biochemistry and Molecular Biology, National Chung Hsing University) and his lab member, Mr. Che-Pei Cho, for their help in accessing the facility to perform isotope-labeling experiments.

This work is supported by the Columbus Young Scholar Fellowship (MOST 109-2636-B-006–005; MOST 110-2636-B-006-010; MOST 111-2636-B-006-013; NSTC 112-2636-B-006-009) from the Ministry of Science and Technology and National Science and Technology Council, Taiwan (to C.-H.Y.). S.-C.C. is supported by the program of the Research Center for Epidemic Prevention Science (MOST

111-2321-B-006–009). The National Cheng Kung University, Taiwan, and Higher Education Sprout Project, Ministry of Education to the Headquarters of the University, Taiwan, also provide funding.

AUTHOR CONTRIBUTIONS

S.-H.H.: Conceptualization, Methodology, Investigation, Validation, Writing-Original Draft. S.-C.C.: Methodology, Writing – Review & Editing. T.-Y.W. & C.-Y.C.: Materials. C.-H.Y.: Conceptualization, Supervision, Writing – Review & Editing, Project administration, Funding acquisition.

DECLARATION OF INTERESTS

C.-Y.C. is the co-founder and shareholder of YD Biolabs, Ltd. T.-Y.W. is an employee of YD Biolabs, Ltd.

INCLUSION AND DIVERSITY

We support inclusive, diverse, and equitable conduct of research.

Received: May 12, 2023
Revised: September 13, 2023
Accepted: November 16, 2023
Published: November 19, 2023

REFERENCES

1. Wen, J.D., Lancaster, L., Hodges, C., Zeri, A.C., Yoshimura, S.H., Noller, H.F., Bustamante, C., and Tinoco, I. (2008). Following translation by single ribosomes one codon at a time. Nature *452*, 598–603.
2. Ellis, N., and Gallant, J. (1982). An Estimate of the Global Error Frequency in Translation. MolMol. Gen. Genet. *188*, 169–172.
3. Gesteland, R.F., Weiss, R.B., and Atkins, J.F. (1992). Recoding - Reprogrammed Genetic Decoding. Science *257*, 1640–1641.
4. Dever, T.E., Dinman, J.D., and Green, R. (2018). Translation Elongation and Recoding in Eukaryotes. Cold Spring Harb Perspect Biol *10*.
5. Rodnina, M.V., Korniy, N., Klimova, M., Karki, P., Peng, B.Z., Senyushkina, T., Belardinelli, R., Maracci, C., Wohlgemuth, I., Samatova, E., and Peske, F. (2020). Translational recoding: canonical translation mechanisms reinterpreted. Nucleic Acids Res. *48*, 1056–1067.
6. Atkins, J.F., Loughran, G., Bhatt, P.R., Firth, A.E., and Baranov, P.V. (2016). Ribosomal frameshifting and transcriptional slippage: From genetic steganography and cryptography to adventitious use. Nucleic Acids Res. *44*, 7007–7078.
7. Weiss, R.B., Dunn, D.M., Atkins, J.F., and Gesteland, R.F. (1987). Slippery Runs, Shifty Stops, Backward Steps, and Forward Hops - -2, -1, +1, +2, +5, and +6 Ribosomal Frameshifting. Cold Spring Harb Sym *52*, 687–693.
8. Fang, Y., et al. (2012). Efficient-2 frameshifting by mammalian ribosomes to synthesize an additional arterivirus protein. P Natl Acad Sci USA *109*, E2920–E2928.
9. Yan, S., Wen, J.D., Bustamante, C., and Tinoco, I. (2015). Ribosome Excursions during mRNA Translocation Mediate Broad Branching of Frameshift Pathways. Cell *160*, 870–881.
10. Clare, J., and Farabaugh, P. (1985). Nucleotide-Sequence of a Yeast Ty Element - Evidence for an Unusual Mechanism of Gene-Expression. P Natl Acad Sci USA *82*, 2829–2833.
11. Ivanov, I.P., and Atkins, J.F. (2007). Ribosomal frameshifting in decoding antizyme mRNAs from yeast and protists to humans: close to 300 cases reveal remarkable diversity despite underlying conservation. Nucleic Acids Res. *35*, 1842–1858.
12. Advani, V.M., and Dinman, J.D. (2016). Reprogramming the genetic code: The emerging role of ribosomal frameshifting in regulating cellular gene expression. Bioessays. *38*, 21–26.
13. Korniy, N., Samatova, E., Anokhina, M.M., Peske, F., and Rodnina, M.V. (2019). Mechanisms and biomedical implications of-1 programmed ribosome frameshifting on viral and bacterial mRNAs. Febs Lett *593*, 1468–1482.
14. Riegger, R.J., and Caliskan, N. (2022). Thinking Outside the Frame: Impacting Genomes Capacity by Programmed Ribosomal Frameshifting. Front. Mol. Biosci. *9*, 842261.
15. Hung, M., Patel, P., Davis, S., and Green, S.R. (1998). Importance of ribosomal frameshifting for human immunodeficiency virus type 1 particle assembly and replication. J. Virol. *72*, 4819–4824.
16. Plant, E.P., Rakauskaite, R., Taylor, D.R., and Dinman, J.D. (2010). Achieving a Golden Mean: Mechanisms by Which Coronaviruses Ensure Synthesis of the Correct Stoichiometric Ratios of Viral Proteins. J. Virol. *84*, 4330–4340.
17. Sun, Y., et al. (2021). Restriction of SARS-CoV-2 replication by targeting programmed-1 ribosomal frameshifting. P Natl Acad Sci USA *118*. e2023051118.
18. Brierley, I., Jenner, A.J., and Inglis, S.C. (1992). Mutational Analysis of the Slippery-Sequence Component of a Coronavirus Ribosomal Frameshifting Signal. J. Mol. Biol. *227*, 463–479.
19. Giedroc, D.P., and Cornish, P.V. (2009). Frameshifting RNA pseudoknots: Structure and mechanism. Virus Res. *139*, 193–208.
20. Lin, Z., Gilbert, R.J.C., and Brierley, I. (2012). Spacer-length dependence of programmed-1 or-2 ribosomal frameshifting on a U(6)A heptamer supports a role for messenger RNA (mRNA) tension in frameshifting. Nucleic Acids Res. *40*, 8674–8689.
21. Yu, C.H., Teulade-Fichou, M.P., and Olsthoorn, R.C.L. (2014). Stimulation of ribosomal frameshifting by RNA G-quadruplex structures. Nucleic Acids Res. *42*, 1887–1892.
22. Caliskan, N., Katunin, V.I., Belardinelli, R., Peske, F., and Rodnina, M.V. (2014). Programmed-1 Frameshifting by Kinetic Partitioning during Impeded Translocation. Cell *157*, 1619–1631.
23. Chen, J., Petrov, A., Johansson, M., Tsai, A., O'Leary, S.E., and Puglisi, J.D. (2014). Dynamic pathways of -1 translational frameshifting. Nature *512*, 328–332.
24. Kim, H.K., et al. (2014). A frameshifting stimulatory stem loop destabilizes the hybrid state and impedes ribosomal translocation. Proc. Natl. Acad. Sci. USA *111*, 5538–5543.
25. Chen, G., Chang, K.Y., Chou, M.Y., Bustamante, C., and Tinoco, I. (2009). Triplex structures in an RNA pseudoknot enhance mechanical stability and increase efficiency of-1 ribosomal frameshifting. P Natl Acad Sci USA *106*, 12706–12711.
26. Yu, C.H., Noteborn, M.H.M., and Olsthoorn, R.C.L. (2010). Stimulation of ribosomal frameshifting by antisense LNA. Nucleic Acids Res. *38*, 8277–8283.
27. Yu, C.H., Noteborn, M.H., Pleij, C.W.A., and Olsthoorn, R.C.L. (2011). Stem-loop structures can effectively substitute for an RNA pseudoknot in-1 ribosomal frameshifting. Nucleic Acids Res. *39*, 8952–8959.
28. Halma, M.T.J., Ritchie, D.B., Cappellano, T.R., Neupane, K., and Woodside, M.T. (2019). Complex dynamics under tension in a high-efficiency frameshift stimulatory structure. Proc. Natl. Acad. Sci. USA *116*, 19500–19505.
29. Larsen, B., Wills, N.M., Gesteland, R.F., and Atkins, J.F. (1994). rRNA-mRNA base pairing stimulates a programmed -1 ribosomal frameshift. J. Bacteriol. *176*, 6842–6851.
30. Su, M.C., Chang, C.T., Chu, C.H., Tsai, C.H., and Chang, K.Y. (2005). An atypical RNA pseudoknot stimulator and an upstream attenuation signal for -1 ribosomal frameshifting of SARS coronavirus. Nucleic Acids Res. *33*, 4265–4275.

31. Craigen, W.J., and Caskey, C.T. (1986). Expression of peptide chain release factor 2 requires high-efficiency frameshift. Nature *322*, 273–275.
32. Baranov, P.V., Gesteland, R.F., and Atkins, J.F. (2002). Release factor 2 frameshifting sites in different bacteria. EMBO Rep. *3*, 373–377.
33. Matsufuji, S., et al. (1995). Autoregulatory frameshifting in decoding mammalian ornithine decarboxylase antizyme. Cell *80*, 51–60.
34. ten Dam, E.B., Pleij, C.W., and Bosch, L. (1990). RNA pseudoknots: translational frameshifting and readthrough on viral RNAs. Virus Genes *4*, 121–136.
35. Li, Y., et al. (2014). Transactivation of programmed ribosomal frameshifting by a viral protein. Proc. Natl. Acad. Sci. USA *111*, E2172–E2181.
36. Napthine, S., Treffers, E.E., Bell, S., Goodfellow, I., Fang, Y., Firth, A.E., Snijder, E.J., and Brierley, I. (2016). A novel role for poly(C) binding proteins in programmed ribosomal frameshifting. Nucleic Acids Res. *44*, 5491–5503.
37. Wang, X., Xuan, Y., Han, Y., Ding, X., Ye, K., Yang, F., Gao, P., Goff, S.P., and Gao, G. (2019). Regulation of HIV-1 Gag-Pol Expression by Shiftless, an Inhibitor of Programmed-1 Ribosomal Frameshifting. Cell *176*, 625–635.e14.
38. Zimmer, M.M., Kibe, A., Rand, U., Pekarek, L., Ye, L., Buck, S., Smyth, R.P., Cicin-Sain, L., and Caliskan, N. (2021). The short isoform of the host antiviral protein ZAP acts as an inhibitor of SARS-CoV-2 programmed ribosomal frameshifting. Nat. Commun. *12*, 7193.
39. Napthine, S., Hill, C.H., Nugent, H.C.M., and Brierley, I. (2021). Modulation of Viral Programmed Ribosomal Frameshifting and Stop Codon Readthrough by the Host Restriction Factor Shiftless. Viruses *13*, 1230.
40. Napthine, S., Ling, R., Finch, L.K., Jones, J.D., Bell, S., Brierley, I., and Firth, A.E. (2017). Protein-directed ribosomal frameshifting temporally regulates gene expression. Nat. Commun. *8*, 15582.
41. Hill, C.H., et al. (2021). Investigating molecular mechanisms of 2A-stimulated ribosomal pausing and frameshifting in Theilovirus. Nucleic Acids Res. *49*, 11938–11958.
42. Hill, C.H., Pekarek, L., Napthine, S., Kibe, A., Firth, A.E., Graham, S.C., Caliskan, N., and Brierley, I. (2021). Structural and molecular basis for Cardiovirus 2A protein as a viral gene expression switch. Nat. Commun. *12*, 7166.
43. Henderson, C.M., Anderson, C.B., and Howard, M.T. (2006). Antisense-induced ribosomal frameshifting. Nucleic Acids Res. *34*, 4302–4310.
44. Howard, M.T., Gesteland, R.F., and Atkins, J.F. (2004). Efficient stimulation of site-specific ribosome frameshifting by antisense oligonucleotides. Rna *10*, 1653–1661.
45. Olsthoorn, R.C., et al. (2004). Novel application of sRNA: stimulation of ribosomal frameshifting. Rna *10*, 1702–1703.
46. Nidhi, S., Anand, U., Oleksak, P., Tripathi, P., Lal, J.A., Thomas, G., Kuca, K., and Tripathi, V. (2021). Novel CRISPR-Cas Systems: An Updated Review of the Current Achievements, Applications, and Future Research Perspectives. Int. J. Mol. Sci. *22*, 3327.
47. Li, J.C., et al. (2022). Discovery of the Rnase activity of CRISPR-Cas12a and its distinguishing cleavage efficiency on various substrates. Chem Commun *58*, 2540–2543.
48. Chen, J.S., Ma, E., Harrington, L.B., Da Costa, M., Tian, X., Palefsky, J.M., and Doudna, J.A. (2018). CRISPR-Cas12a target binding unleashes indiscriminate single-stranded DNase activity. Science *360*, 436–439.
49. Strutt, S.C., Torrez, R.M., Kaya, E., Negrete, O.A., and Doudna, J.A. (2018). RNA-dependent RNA targeting by CRISPR-Cas9. Elife *7*, e32724.
50. Xu, S., Luk, K., Yao, Q., Shen, A.H., Zeng, J., Wu, Y., Luo, H.Y., Brendel, C., Pinello, L., Chui, D.H.K., et al. (2019). Editing aberrant splice sites efficiently restores beta-globin expression in beta-thalassemia. Blood *133*, 2255–2262.
51. Zetsche, B., Heidenreich, M., Mohanraju, P., Fedorova, I., Kneppers, J., DeGennaro, E.M., Winblad, N., Choudhury, S.R., Abudayyeh, O.O., Gootenberg, J.S., et al. (2017). Multiplex gene editing by CRISPR-Cpf1 using a single crRNA array (vol 35, pg 31, 2017). Nat. Biotechnol. *35*, 178.
52. Somogyi, P., Jenner, A.J., Brierley, I., and Inglis, S.C. (1993). Ribosomal Pausing during Translation of an Rna Pseudoknot. Mol. Cell Biol. *13*, 6931–6940.
53. Rodrigo, C.M., Cencic, R., Roche, S.P., Pelletier, J., and Porco, J.A. (2012). Synthesis of Rocaglamide Hydroxamates and Related Compounds as Eukaryotic Translation Inhibitors: Synthetic and Biological Studies. J. Med. Chem. *55*, 558–562.
54. Mouzakis, K.D., Lang, A.L., Vander Meulen, K.A., Easterday, P.D., and Butcher, S.E. (2013). HIV-1 frameshift efficiency is primarily determined by the stability of base pairs positioned at the mRNA entrance channel of the ribosome. Nucleic Acids Res. *41*, 1901–1913.
55. Plant, E.P., Sims, A.C., Baric, R.S., Dinman, J.D., and Taylor, D.R. (2013). Altering SARS Coronavirus Frameshift Efficiency Affects Genomic and Subgenomic RNA Production. Viruses-Basel *5*, 279–294.
56. O'Connell, M.R., Oakes, B.L., Sternberg, S.H., East-Seletsky, A., Kaplan, M., and Doudna, J.A. (2014). Programmable RNA recognition and cleavage by CRISPR/Cas9. Nature *516*, 263–266.
57. Zhang, K., Zheludev, I.N., Hagey, R.J., Haslecker, R., Hou, Y.J., Kretsch, R., Pintilie, G.D., Rangan, R., Kladwang, W., Li, S., et al. (2021). Cryo-EM and antisense targeting of the 28-kDa frameshift stimulation element from the SARS-CoV-2 RNA genome. NatNat. Struct. Mol. Biol. *28*, 747–754.
58. Kelly, J.A., Olson, A.N., Neupane, K., Munshi, S., San Emeterio, J., Pollack, L., Woodside, M.T., and Dinman, J.D. (2020). Structural and functional conservation of the programmed -1 ribosomal frameshift signal of SARS coronavirus 2 (SARS-CoV-2). J. Biol. Chem. *295*, 10741–10748.
59. Roman, C., Lewicka, A., Koirala, D., Li, N.S., and Piccirilli, J.A. (2021). The SARS-CoV-2 Programmed -1 Ribosomal Frameshifting Element Crystal Structure Solved to 2.09 A Using Chaperone-Assisted RNA Crystallography. ACS Chem. Biol. *16*, 1469–1481.
60. Jones, C.P., and Ferré-D'Amaré, A.R. (2022). Crystal structure of the severe acute respiratory syndrome coronavirus 2 (SARS-CoV-2) frameshifting pseudoknot. RNA *28*, 239–249.
61. Bhatt, P.R., Scaiola, A., Loughran, G., Leibundgut, M., Kratzel, A., Meurs, R., Dreos, R., O'Connor, K.M., McMillan, A., Bode, J.W., et al. (2021). Structural basis of ribosomal frameshifting during translation of the SARS-CoV-2 RNA genome. Science *372*, 1306–1313.
62. Lorenz, R., Bernhart, S.H., Höner zu Siederdissen, C., et al. (2011). ViennaRNA Package 2.0. Algorithms Mol Biol *6*, 26.
63. Plant, E.P., Pérez-Alvarado, G.C., Jacobs, J.L., Mukhopadhyay, B., Hennig, M., and Dinman, J.D. (2005). A three-stemmed mRNA pseudoknot in the SARS coronavirus frameshift signal. PLoS Biol. *3*, e172-1023.
64. Chen, Y.T., Chang, K.C., Hu, H.T., Chen, Y.L., Lin, Y.H., Hsu, C.F., Chang, C.F., Chang, K.Y., and Wen, J.D. (2017). Coordination among tertiary base pairs results in an efficient frameshift-stimulating RNA pseudoknot. Nucleic Acids Res. *45*, 6011–6022.
65. Olsthoorn, R.C.L., Reumerman, R., Hilbers, C.W., Pleij, C.W.A., and Heus, H.A. (2010). Functional analysis of the SRV-1 RNA frameshifting pseudoknot. Nucleic Acids Res. *38*, 7665–7672.
66. Nikolic, E.I.C., King, L.M., Vidakovic, M., Irigoyen, N., and Brierley, I. (2012). Modulation of ribosomal frameshifting frequency and its effect on the replication of Rous sarcoma virus. J. Virol. *86*, 11581–11594.
67. Brakier-Gingras, L., Charbonneau, J., and Butcher, S.E. (2012). Targeting frameshifting in the human immunodeficiency virus. Expert Opin. Ther. Targets *16*, 249–258.
68. Grentzmann, G., Ingram, J.A., Kelly, P.J., Gesteland, R.F., and Atkins, J.F. (1998). A dual-luciferase reporter system for studying recoding signals. Rna *4*, 479–486.
69. Biswas, P., Jiang, X., Pacchia, A.L., Dougherty, J.P., and Peltz, S.W. (2004). The human immunodeficiency virus type 1 ribosomal frameshifting site is an invariant sequence determinant and an important target for antiviral therapy. J. Virol. *78*, 2082–2087.
70. Theis, C., Reeder, J., and Giegerich, R. (2008). KnotInFrame: prediction of -1 ribosomal frameshift events. Nucleic Acids Res. *36*, 6013–6020.
71. Moon, S., Byun, Y., Kim, H.J., Jeong, S., and Han, K. (2004). Predicting genes expressed via -1 and +1 frameshifts. Nucleic Acids Res. *32*, 4884–4892.
72. Schlick, T., Zhu, Q., Dey, A., Jain, S., Yan, S., and Laederach, A. (2021). To Knot or Not to Knot: Multiple Conformations of the SARS-CoV-2 Frameshifting RNA Element. JJ. Am. Chem. Soc. *143*, 11404–11422.
73. Iwakawa, H.O., Lam, A.Y.W., Mine, A., Fujita, T., Kiyokawa, K., Yoshikawa, M., Takeda, A., Iwasaki, S., and Tomari, Y. (2021). Ribosome stalling caused by the Argonaute-microRNA-SGS3 complex regulates the production of secondary siRNAs in plants. Cell Rep. *35*, 109300.
74. Zhang, K., Zhang, X., Cai, Z., Zhou, J., Cao, R., Zhao, Y., Chen, Z., Wang, D., Ruan, W., Zhao, Q., et al. (2018). A novel class of microRNA-recognition elements that function only within open reading frames. NatNat. Struct. Mol. Biol. *25*, 1019–1027.
75. Chung, B.Y.W., Firth, A.E., and Atkins, J.F. (2010). Frameshifting in Alphaviruses: A Diversity of 3 ' Stimulatory Structures. J. Mol. Biol. *397*, 448–456.
76. Belew, A.T., Meskauskas, A., Musalgaonkar, S., Advani, V.M., Sulima, S.O., Kasprzak, W.K., Shapiro, B.A., and Dinman, J.D. (2014). Ribosomal frameshifting in the CCR5 mRNA is regulated by miRNAs and the NMD pathway. Nature *512*, 265–269.

77. Khan, Y.A., Loughran, G., Steckelberg, A.L., Brown, K., Kiniry, S.J., Stewart, H., Baranov, P.V., Kieft, J.S., Firth, A.E., and Atkins, J.F. (2022). Evaluating ribosomal frameshifting in *CCR5* mRNA decoding. Nature *604*, E16–E23.
78. Mikl, M., Pilpel, Y., and Segal, E. (2020). High-throughput interrogation of programmed ribosomal frameshifting in human cells. Nat. Commun. *11*, 3061.
79. Matsumoto, S., Caliskan, N., Rodnina, M.V., Murata, A., and Nakatani, K. (2018). Small synthetic molecule-stabilized RNA pseudoknot as an activator for-1 ribosomal frameshifting. Nucleic Acids Res. *46*, 8079–8089.
80. Haniff, H.S., et al. (2020). Targeting the SARS-CoV-2 RNA Genome with Small Molecule Binders and Ribonuclease Targeting Chimera (RIBOTAC) Degraders. Acs Central Sci *6*, 1713–1721.
81. Munshi, S., Neupane, K., Ileperuma, S.M., Halma, M.T.J., Kelly, J.A., Halpern, C.F., Dinman, J.D., Loerch, S., and Woodside, M.T. (2022). Identifying Inhibitors of-1 Programmed Ribosomal Frameshifting in a Broad Spectrum of Coronaviruses. Viruses *14*, 177.
82. Marcheschi, R.J., Mouzakis, K.D., and Butcher, S.E. (2009). Selection and Characterization of Small Molecules That Bind the HIV-1 Frameshift Site RNA. ACS Chem. Biol. *4*, 844–854.
83. Pekarek, L., Zimmer, M.M., Gribling-Burrer, A.S., Buck, S., Smyth, R., and Caliskan, N. (2023). Cis-mediated interactions of the SARS-CoV-2 frameshift RNA alter its conformations and affect function. Nucleic Acids Res. *51*, 728–743.
84. Crooke, S.T., Liang, X.H., Baker, B.F., and Crooke, R.M. (2021). Antisense technology: A review. J. Biol. Chem. *296*, 100416.
85. Jeon, Y., Choi, Y.H., Jang, Y., Yu, J., Goo, J., Lee, G., Jeong, Y.K., Lee, S.H., Kim, I.S., Kim, J.S., et al. (2018). Direct observation of DNA target searching and cleavage by CRISPR-Cas12a. Nat. Commun. *9*, 2777.
86. Liang, X.H., Sun, H., Nichols, J.G., and Crooke, S.T. (2017). RNase H1-Dependent Antisense Oligonucleotides Are Robustly Active in Directing RNA Cleavage in Both the Cytoplasm and the Nucleus. Mol. Ther. *25*, 2075–2092.
87. Raguram, A., Banskota, S., and Liu, D.R. (2022). Therapeutic in vivo delivery of gene editing agents. Cell *185*, 2806–2827.
88. Rapireddy, S., He, G., Roy, S., Armitage, B.A., and Ly, D.H. (2007). Strand invasion of mixed-sequence B-DNA by acridine-linked, gamma-peptide nucleic acid (gamma-PNA). JJ. Am. Chem. Soc. *129*, 15596–15600.
89. Yu, A.M., et al. (2021). Computationally reconstructing cotranscriptional RNA folding from experimental data reveals rearrangement of non-native folding intermediates. Mol. Cell *81*, 870.
90. Yu, D., Han, H.J., Yu, J., Kim, J., Lee, G.H., Yang, J.H., Song, B.M., Tark, D., Choi, B.S., Kang, S.M., and Heo, W.D. (2023). Pseudoknot-targeting Cas13b combats SARS-CoV-2 infection by suppressing viral replication. Mol. Ther. *31*, 1675–1687.
91. Tsai, S.Q., Zheng, Z., Nguyen, N.T., Liebers, M., Topkar, V.V., Thapar, V., Wyvekens, N., Khayter, C., Iafrate, A.J., Le, L.P., et al. (2015). GUIDE-seq enables genome-wide profiling of off-target cleavage by CRISPR-Cas nucleases. Nat. Biotechnol. *33*, 187–197.

STAR★METHODS

KEY RESOURCES TABLE

REAGENT or RESOURCE	SOURCE	IDENTIFIER
Antibodies		
Mouse monoclonal anti-HA-tag (F-7)	Santa Cruz Biotechnology	Cat# sc-7392; RRID: AB_627809
Bacterial and virus strains		
Stable Competent *E. coli*	New England Biolabs	Cat# C3040I
E. coli DH5α	N/A	N/A
Chemicals, peptides, and recombinant proteins		
CR-1-31-B (CR-31)	MedChemExpress	Cat# HY-136453
isopropyl β-D-1-thiogalactopyranoside (IPTG)	Sigma	Cat# 367-93-1
Recombinant LbCas12a-3HA-6His	This paper	N/A
Recombinant MBP-dCas9	This paper, MR O'Connell et al.[50]	Addgene ID: #60815
Murine RNase Inhibitor	Vazyme Biotech	Cat# R301
RNase A	VWR International	Cat# 97062-172
Q5 DNA Polymerase	New England Biolabs	Cat# M0491S
T4 DNA Ligase	New England Biolabs	Cat# M0202L
T4 Polynucleotide Kinase	New England Biolabs	Cat# M0201L
HiFi DNA Assembly Cloning Kit	New England Biolabs	Cat# E5520S
T7 RNA Polymerase	New England Biolabs	Cat# E2040S
SP6 RNA Polymerase	New England Biolabs	Cat# E2070S
Anti-Reverse Cap Analog (ARCA)	New England Biolabs	Cat# S1411S
EasyTag L-[^{35}S]-Methionine	Perkin Elmer	Cat# NEG709A005UC
Lipofectamine 3000	Thermo Fisher Scientific	Cat# L3000008
SYBR Gold	Thermo Fisher Scientific	Cat# S11494
Urea	Cytiva	Cat# 17-1319-01
Critical commercial assays		
Phosphorimager screen	Amersham	
Rabbit Reticulocyte Lysate	Promega	Cat# L4960
Luciferase Assay System	Promega	Cat# E2940
Experimental models: Cell lines		
HEK293T	ATCC	Cat# CRL-3216
Oligonucleotides		
Transcription templates (See Table S1)	IDT	N/A
Primers for cloning p2FL-v1, v2, v3,and v4 (See Table S3)	IDT	N/A
Primers for cloning p2FL_3 nts, 5 nts, 9 nts, and 11 nts (See Table S3)	IDT	N/A
Primers for cloning p2FL-SARS CoV2 PK (See Table S3)	IDT	N/A
Primers for cloning pET21a-Cas12a without NLS (See Table S3)	IDT	N/A
Recombinant DNA		
p2FL-v1	This paper	N/A
p2FL-v2	This paper	N/A
p2FL-v3	This paper	N/A

(*Continued on next page*)

Continued

REAGENT or RESOURCE	SOURCE	IDENTIFIER
p2FL-v4	This paper	N/A
p2FL_3 nts	This paper	N/A
p2FL_5 nts	This paper	N/A
p2FL_7 nts	This paper	N/A
p2FL_9 nts	This paper	N/A
p2FL_11 nts	This paper	N/A
p2FL-SARS CoV2 PK	This paper	N/A
p2FL-v1_RT	This paper	N/A
p2FL-control	This paper	N/A
p2FL-HP	This paper	N/A
pET-21a_LbCas12a-2xNLS-3HA-6His	P Liu et al., 2019[49]	Addgene ID: #114366
pET-21a_LbCas12a-3HA-6His	This paper	N/A
Software and algorithms		
ViennaRNA Web Services	Institute for Theoretical Chemistry, University of Vienna	http://rna.tbi.univie.ac.at/

RESOURCE AVAILABILITY

Lead contact

Further information and requests for resources and reagents should be directed to and will be fulfilled by the lead contact, Chien-Hung Yu (chienhung_yu@mail.ncku.edu.tw).

Materials availability

This study did not generate new unique reagents.

Data and code availability

- All data reported in this paper will be shared by the lead contact upon request.
- This paper does not report original code.
- Any additional information required to reanalyze the data reported in this paper is available from the lead contact upon request.

EXPERIMENTAL MODEL AND STUDY PARTICIPANT DETAILS

HEK293T was purchased from the American Type Culture Collection (ATCC). HEK293T cells (ATCC, CRL-3216) are female in origin. This Cell line was not authenticated internally. The cells were tested and confirmed to be free of mycoplasma by ATCC.

METHOD DETAILS

Plasmid construction

The p2FL constructs were generated based on the reported SF reporter plasmid.[26] The original influenza polymerase basic 2 (PB2) was replaced by eGFP (abbreviated as GFP) and mDsRed (abbreviated as RFP) (a gift from Dr. Hua-Lin Wu, National Cheng Kung University). In this newly constructed p2FL plasmid, GFP would be produced in 0 frame and RFP in −1 frame. The slippery sequence, spacer (3, 5, 7, 9, 11 nts), and targeting sequences (v1, v2, v3, v4, SARS CoV2 PK) were cloned between GFP and RFP of p2FL using standard cloning or NEBuilder HiFi DNA Assembly (NEB). The p2Luc-SARS CoV2 PK plasmid was created by inserting SARS-CoV-2 frameshifting context into p2Luc[68] (a gift from Dr. Atkins, University College Cork) through NEBuilder HiFi DNA Assembly (NEB). The pET-21a_LbCas12a-3HA-6His was generated by PCR-mediated deletion from Addgene plasmids pET-21a_LbCas12a-2xNLS-3HA-6His[50] (#114366). The constructs are confirmed by Sanger sequencing (Genomics, Taiwan). Please see Table S3 for the detail oligonucleotide sequences.

In vitro transcription

The DNA templates for *in vitro* transcription were PCR amplified from indicated p2FL and p2Luc series plasmids. The SP6 RNA polymerase (NEB) was used to transcribe p2FL series templates; T7 RNA polymerase (NEB) was used to transcribe p2luc series templates. The mRNA transcription protocol was based on standard RNA synthesis, and the capped mRNA was transcribed using the manufacturer's Anti-Reverse Cap Analog (ARCA, NEB) RNA synthesis protocol. The crRNAs and sgRNA templates were annealed by two DNA oligonucleotides (IDT), containing a wholly matched T7 promoter region and a single-stranded template region. Subsequently, crRNAs were synthesized using

a short template RNA synthesis protocol (NEB). RNA products were purified by LiCl precipitation followed by urea PAGE to confirm the integrity. The complete list of the DNA oligonucleotide sequences is in the supplementary materials (Table S1).

Expression and purification of Cas12a

E. coli Acella cells containing the pET-21a_LbCas12a-3HA-6His were grown in the 2 L of LB medium supplemented with 0.5% glucose and 50 μg/mL Ampicillin at 37°C. When the cell density reached 0.6–0.8 absorbance at the OD_{600}, 1mM of isopropyl β-D-1-thiogalactopyranoside (IPTG) was added into the culture. Cells were allowed to grow for an additional 4 h at 37°C, then harvested by centrifugation at 7000×g for 10 min at 4°C. The cell pellets were resuspended with the Tag Buffer A [50 mM Tris-HCl (pH 8.0), 100 mM NaCl, 1 mM EDTA, 1 mM DTT, 5% (v/v) glycerol] containing 1 mM Benzamidine hydrochloride, and lysed by the sonication. Cell lysates were clarified by centrifugation at 18,000×g for 20 min at 4°C. A final concentration of 0.3% (w/v) polyethyleneimine and 800 mM NaCl were added to the cell lysate to remove nucleic acids. The cell lysates were clarified by centrifugation at 18,000×g for 20 min at 4°C. The ammonium sulfate was added (to the 60% saturation) into the combined supernatant. The protein precipitates were obtained by centrifugation at 18,000×g for 20 min at 4°C. The protein precipitates were first suspended with the Ni-NTA Buffer A without NaCl [50 mM Tris-HCl (pH 8.0), 20 mM imidazole, 1 mM EDTA, 1 mM DTT, 5% (v/v) glycerol] and clarified by centrifugation at 18,000×g for 20 min at 4°C. The supernatant was further diluted with the Ni-NTA Buffer A and directed loaded onto a 5mL of HisTrap HP column pre-equilibrated in the Ni-NTA Buffer A [50 mM Tris-HCl (pH 8.0), 20 mM imidazole, 500 mM NaCl, 1 mM EDTA, 1 mM DTT, 5% (v/v) glycerol]. The protein was eluted with a linear 20–500 mM imidazole gradient using the Ni-NTA Buffer A and Buffer B [50 mM Tris-HCl (pH 8.0), 500 mM imidazole, 500 mM NaCl, 1 mM EDTA, 1 mM DTT, 5% (v/v) glycerol]. The protein elution fractions were analyzed by the 10% SDS-PAGE. Fractions containing Cas12a protein were pooled and dialyzed at 4°C overnight against the dialysis buffer [50 mM Tris-HCl (pH 8.0), 300 mM NaCl, 1 mM EDTA, 1 mM DTT, 5% (v/v) glycerol]. The sample was diluted with the Tag Buffer A and loaded onto a 5 mL of HiTrap Heparin HP column pre-equilibrated with the Tag Buffer A. The protein was eluted with a linear 100–1000 mM NaCl gradient using the Tag Buffer A and Buffer B [50 mM Tris-HCl (pH 8.0), 1M NaCl, 1 mM EDTA, 1 mM DTT, 5% (v/v) glycerol]. The elution fractions were analyzed by the 10% SDS-PAGE. Fractions containing Cas12a protein were pooled and loaded onto a HiPrep 26/60 Sephacryl S-200HR column pre-equilibrated and eluted with the Tag Buffer A. The protein elution fractions were analyzed by the 10% SDS-PAGE. Fractions containing Cas12a were pooled and stored in the 40% glycerol at −20°C. The final protein concentration was determined by the Bradford Assay using bovine serum albumin (BSA) as the standard.

Expression and purification of dCas9

E. coli Acella cells containing the MBP-dCas9 (Addgene, #60815[56]) were grown in the 2 L of LB medium supplemented with 0.5% glucose and 50 μg/mL Ampicillin at 18°C. When the cell density reached 0.6–0.8 absorbance at the OD_{600}, 1 mM of IPTG was added into the culture. Cells were allowed to grow for an additional 16 h at 18°C, then harvested by centrifugation at 7000×g for 10 min at 4°C. The cell pellets were resuspended with the Tag Buffer A [50 mM Tris-HCl (pH 8.0), 100 mM NaCl, 1 mM EDTA, 1mM DTT, 5% (v/v) glycerol] containing 1 mM Benzamidine hydrochloride, and lysed by the sonication. Cell lysates were clarified by centrifugation at 18,000×g for 20 min at 4°C. A final concentration of 0.3% (w/v) polyethyleneimine and 800 mM NaCl were added to the cell lysate to remove nucleic acids. The cell lysates were clarified by centrifugation at 18,000×g for 20 min at 4°C. The ammonium sulfate was added (to the 60% saturation) into the combined supernatant. The protein precipitates were obtained by centrifugation at 18,000×g for 20 min at 4°C. The protein precipitates were first suspended with the Amylose Buffer A without NaCl [20 mM Tris-HCl (pH 7.5), 1 mM EDTA, 5% (v/v) glycerol] and clarified by centrifugation at 18,000×g for 20 min at 4°C. The supernatant was further diluted with the Amylose Buffer A and directed loaded onto a 10mL of Amylose resin pre-equilibrated in the Amylose Buffer A [20 mM Tris-HCl (pH 7.5), 200 mM NaCl, 1mM EDTA, 5% (v/v) glycerol]. The protein was eluted with the Amylose Buffer B [20 mM Tris-HCl (pH 7.5), 200 mM NaCl, 1 mM EDTA, 20 mM Maltose, 5% (v/v) glycerol]. The protein elution fractions were analyzed by the 10% SDS-PAGE. Fractions containing Cas9 protein were pooled and dialyzed at 4°C overnight against the dialysis buffer [50 mM Tris-HCl (pH 8.0), 300 mM NaCl, 1 mM EDTA, 1 mM DTT, 5% (v/v) glycerol]. The sample was diluted with the Ni-NTA Buffer A without NaCl and loaded onto a 5 mL of HisTrap HP column pre-equilibrated with the Ni-NTA Buffer A [50 mM Tris-HCl (pH 8.0), 500 mM NaCl, 20 mM Imidazole, 1 mM EDTA, 1 mM DTT, 5% (v/v) glycerol]. The protein was eluted with a linear 20–500 mM Imidazole gradient using the Ni-NTA Buffer A and Buffer B [50 mM Tris-HCl (pH 8.0), 500 mM NaCl, 500 mM Imidazole, 1 mM EDTA, 1 mM DTT, 5% (v/v) glycerol]. The elution fractions were analyzed by the 10% SDS-PAGE. Fractions containing Cas9 were pooled and stored in the 50% glycerol at −20°C. The final protein concentration was determined by the Bradford Assay using BSA as the standard.

Electrophoretic mobility shift assay (EMSA)

The 55 pmol crRNA was incubated with 50 pmol Cas12a in 1x complex reconstitution buffer (20 mM HEPES, pH 7.5, 250 mM KCl, 2 mM MgCl) at room temperature for 10 min. After mixing 500 ng of mRNA with crRNA and Cas12a-crRNA complex, respectively, the mixtures were added to an equal volume of 2x EMSA loading dye (20% glycerol, 0.025% bromophenol blue, 0.025% xylene cyanol FF, 1 mM EDTA) and analyzed on 1% agarose gel.

Cas12a RNA cleavage activity assay

The 55 pmol crRNA was incubated with 50 pmol Cas12a for 10 min at room temperature in 1x complex reconstitution buffer. The complexes were mixed with 500 ng of mRNA for an additional 10 min at room temperature. The reactions were then mixed with 2x RNA loading dye

(95% formamide, 0.025% SDS, 0.025% bromophenol blue, 0.025% xylene cyanol FF, 1 mM EDTA) and incubated at 90°C for 5 min to denature. The mixtures were subsequently chilled on ice, centrifuged, and the chilled were loaded onto a 1% agarose gel for staining.

RNase protection assay

The amount of 22 pmol of crRNA was incubated with 20 pmol Cas12a in 1x complex reconstitution buffer at room temperature for 10 min, followed by adding 100 ng RNase A for 10 min at room temperature. The reactions were then mixed with spike-in control [a synthesized 120 nts single-stranded DNA (ssDNA)]. The mixtures were then purified by phenol-chloroform extraction and ethanol precipitation. The purified mixtures were then mixed with 2x TBE-urea RNA loading dye (80 mM Tris-base, 80 mM boric acid, 2 mM EDTA, 8 M urea, 0.025% bromophenol blue, 0.025% xylene cyanol FF) and incubated at 90°C for 5 min. The samples were then chilled on ice, centrifuged, and resolved on a 12% TBE-Urea PAGE. The PAGE was then visualized by SYBR Gold staining (Invitrogen).

In vitro translation

In vitro translation was conducted using the Rabbit Reticulocyte Lysate System (RRL, Promega). For frameshifting experiments, the 10 μL translation reactions were prepared, containing 4 μL RRL, 4 μM amino acid mixture without methionine, 2 μCi [^{35}S] methionine (PerkinElmer), and the premixed solution of 0.1 pmol mRNA, and 0.1–50 pmol ASO or Cas12a-crRNA complex. The reactions were then incubated for 60 min at 28°C. For ribosomal pausing assays, each 10 μL final translation reaction consisting of 4 μL RRL, 4 μM of amino acid mixture without methionine, 2 μCi methionine, and a premixed solution of 0.2 pmol mRNA, and 10 pmol ASO or Cas12a-crRNA complex. Reactions were initiated at 26°C, and after 5 min, CR-31 (MedChemExpress) was added at a final concentration of 500 nM to inhibit ribosome initiation. At each indicated interval, 9 μL aliquots were removed from the reaction and mixed with 1 μg RNase A for 10 min at room temperature to terminate translation. The samples were mixed with 5x protein sample buffer, heated at 85°C for 5 min, and separated on 12.5% SDS-PAGE. SDS-PAGE gels were fixed on cardstock, dried under vacuum, and exposed to a phosphorimager screen, visualized by Typhoon Storage Phosphorimager equipped with a laser scanner. The in-frames, −1 frameshift, and paused protein products on the radiograph were quantified and estimated by Quantity One (Biorad).

The frameshift percentages were calculated as follows as the formula:

$$\frac{(FS - FS^{BKGD})/N}{\left[\frac{FS - FS^{BKGD}}{N} + \frac{NFS - NFS^{BKGD}}{n}\right]} * \% = \text{frameshift percent}$$

The FS and NFS denote the volume of −1 and 0 frameshift products, respectively. And FS^{BKGD} and NFS^{BKGD} represent the background volume of −1 and 0 frameshift products, respectively. The N and n represent the amount of methionine in a −1 and 0 frameshift product, respectively. An example of −1 PRF efficiency calculation is shown in Figure S6.

In the dual-luciferase frameshifting assay in RRL, the translation reactions were assembled similarly as above, except that [^{35}S] methionine was left out, and the complete amino acid mixture was supplemented. The luciferase activity was measured using Dual-Glo Luciferase Assay Reagent (Promega) on a plate reader (BMG Labtech) according to the manufacturer's protocol. To obtain the −1 PRF efficiency of the dual-luciferase system samples, the *firefly*/*Renilla* activity ratio generated from the control reporter was divided into that from frameshift reporters carrying frameshifting signals of interest and multiplied by 100 to obtain frameshifting efficiencies (expressed as percentages) for each recoding signal.

Cell culture and transfection

HEK293T cells were maintained in DMEM supplemented with 10% FBS and 1% Pen-Strep and were incubated at 37°C with 5% CO2. When the cell density reached 70% confluency, the complete medium was replaced 30 min before transfection. Meanwhile, Lipofectamine 3000 (Invitrogen) was diluted in a serum-free medium, mixed with premixed Cas12a-crRNA-mRNA ternary complex, and then incubated at room temperature for 10 min. The lipoplexes were added dropwise to the cell culture medium. After 8 h, cells were imaged by immunofluorescence imaging or lysed with 5x passive lysis buffer, and the luciferase intensity of the lysates was measured (Dual-Glo Luciferase Assay Reagent, Promega). To obtain the −1 PRF efficiency of the dual-luciferase system samples, the *firefly*/*Renilla* activity ratio generated from the control reporter was divided into that from frameshift reporters carrying frameshifting signals of interest and multiplied by 100 to obtain frameshifting efficiencies (expressed as percentages) for each recoding signal.

Immunofluorescence assay

HEK293T cells were seeded on a 24-well plate. After 18 h, the cells were transiently transfected with Cas12a-crRNA-mRNA ternary complex. Eight hours after transfection, the medium was removed, and the cells were washed with PBS. The cells were then fixed with 4% paraformaldehyde for 10 min at room temperature, permeabilized with 0.25% Triton X-100 for 5 min at room temperature, and blocked in 5% BSA for 1 h at room temperature. The blocked cells were incubated with anti-HA antibody (sc-7392, Santa Cruz Biotechnology) at 1:100 dilution at room temperature for 1 h. After washing three times with PBS, the samples were incubated with the Goat anti-Mouse IgG (H + L) secondary antibody-FITC (#31569, Invitrogen) in the dark for 1 h at room temperature. The samples were washed thrice with PBS and stained with DAPI to

visualize the nuclei. After washing five times, the coverslip samples were placed on microscope slides and dried overnight. The samples were visualized and imaged with fluorescence microscopy (Olympus).

QUANTIFICATION AND STATISTICAL ANALYSIS

The frameshifting efficiency assay was calculated using a paired t-test.

*p value < 0.05; **p value <0.01; ***p value <0.001.